AMERICAN UNIVERSITY OF BEIRUT

PREPARATION OF COLLOIDAL SILICA NANOPARTICLES
FOR ANALYTICAL APPLICATIONS

by
JUSTINE ALBERT DAGHER

A thesis
submitted in partial fulfillment of the requirements
for the degree of Master of Science
to the Department of Chemistry
of the Faculty of Arts and Sciences
at the American University of Beirut

Beirut, Lebanon
January 2022

AMERICAN UNIVERSITY OF BEIRUT

PREPARATION OF COLLOIDAL SILICA NANOPARTICLES FOR ANALYTICAL APPLICATIONS

by
JUSTINE ALBERT DAGHER

Approved by:

_____
Dr. Digambara Patra, Professor   Advisor
Chemistry

_____
Dr. Mohamad Hmadeh, Associate Professor
Chemistry   Member of Committee

_____
Dr. Pierre Karam, Associate Professor
Chemistry   Member of Committee

Date of thesis defense: January 14, 2022

AMERICAN UNIVERSITY OF BEIRUT

THESIS RELEASE FORM

Student Name: _____ Dagher _____ Justine _____ Albert _____
                               Last   First   Middle

I authorize the American University of Beirut, to: (a) reproduce hard or electronic copies of my thesis; (b) include such copies in the archives and digital repositories of the University; and (c) make freely available such copies to third parties for research or educational purposes:

☐ As of the date of submission

☐ One year from the date of submission of my thesis.

☒ Two years from the date of submission of my thesis.

☐ Three years from the date of submission of my thesis.

_____   February 8, 2022
Signature   Date

ACKNOWLEDGEMENTS

ABSTRACT
OF THE THESIS OF

Justine Albert Dagher   for   Master of Science
                                                         Major: Chemistry

Title: Preparation of Colloidal Silica Nanoparticles for Analytical Applications

Colloidal silica or silicon dioxide nanoparticles (SiO_2 NPs) can be obtained in different size ranges and they are recognized by their wide applications. In this work, the synthesis of highly stable SiO_2 NPs in small size range was carried out. Accordingly, the preparation of these nanoparticles was done based on a simple synthesis route, that consist of the hydrolysis of silica colloidal in ethanol medium using ultrasonication by sol-gel process. The size of the NPs and their stability will be controlled by varying the reaction parameters and taking into consideration the silica precursor used and the best concentration of sodium hydroxide. Furthermore, the formed silica powder will be characterized by using microscopic and spectroscopic techniques such as XRD, TGA and SEM. The purpose of this study is the formation of the most suitable, highly stable, small and uniform silica nanoparticles that will be used in various applications.

Firstly, the prepared SiO_2 NPs played an outstanding role as nanoprobe for the detection of silver ion in an easy, fast, cheap, selective and sensitive method using Resonance Rayleigh scattering technique. As the concentration of silver ion increased (5-300 µM) the RRS intensity was seen to decrease. The LOD obtained was equal to 130 nM. The recovery range was between 98.4-100.4%.

Secondly, the adsorption of benzo(ghi)perylene onto the surface of SiO_2 NPs was established with kinetic and isothermal studies. In the first step, a complete study of the adsorption of benzo(ghi)perylene using SiO_2 NPs as adsorbent was verified. The impact of the adsorbent dose, the concentration of the PAH, the pH and the temperature of the solution were varied and regulated in a certain assortment. It was found that the adsorption was improved when increasing the dosage of the nanoparticles and with subsiding the concentration of the PAH. Hence, the numerous adsorption sites will extend to fullness. Additionally, a basic medium improved the adsorption process of benzo(ghi)perylene. Then the kinetics study was investigated, and it was found that the adsorption process followed the 1st order kinetic model which indicated that it was a physisorption. Afterwards the isothermal study was also carried out and showed that the adsorption process followed Langmuir isotherm model. Finally, thermodynamics parameters were calculated, and a negative standard free energy change was acquired in a range of $-20 < \Delta G^o < 0$ kJ/mol indicating that indeed the adsorption process taking place was a physisorption.

Keywords: silica nanoparticles, optimization, silver ion, RRS intensity, adsorption, adsorption capacity, benzo(ghi)perylene, kinetics, isotherms, thermodynamics.

TABLE OF CONTENTS

ILLUSTRATIONS

Figure

7

TABLES

ABBREVIATIONS

Ag^+: Silver ion.
$AgNO_3$: Silver nitrate.
Al^{3+}: Aluminum ion.
APTMS: (3-aminopropyl) triethoxysilane.
BET: Brunauer–Emmett–Teller theory.
Cu^{2+}: Copper ion.
DDW: Double distilled water.
EtOH: Ethanol.
Hg^{2+}: Mercury ion.
K^+: Potassium ion.
LOD: Limit of Detection.
LOQ: Limit of Quantification.
Na^+: Sodium ion.
NaOH: Sodium hydroxide.
Ni^{2+}: Nickel ion.
PAH: Polycyclic aromatic hydrocarbon.
Pb^{2+}: Lead ion.
RRS: Resonance Rayleigh scattering.
SEM: Scanning electron microscopy.
SiO_2 NPs: Silica nanoparticles.
TEOS: Triethyl orthosilicate.
TGA: Thermogravimetric analysis.
UV-Vis: Ultraviolet-visible spectrometry.
XRD: X-Ray Diffractogram.
Zn^{2+}: Zinc ion.

CHAPTER I

INTRODUCTION

A. Nanomaterials

1. Definition

Nanotechnology has emerged hugely in the last couple of years in all fields of research. Nanotechnologies are largely based on nanomaterials and are commercially available as fibers, coatings, etc. [1]. Nanomaterials observed their first ever definition in 2010, and upon the request of the European Commission, by Goran Liden in order for it to be used in the European Union legislation and programed.

Liden's definition recapitulated 3 different points: the size distribution, the surface area and the size of the internal structural element. Therefore, nanomaterial should obey to at least one of the following standards [2]:

- A nanomaterial compound should contain at least one external dimension in the range of 1-100 nm for less than 1% of their relative number size distribution.

- A nanomaterial compound should have a specific surface area less than 60 m^2/cm^{-3} if its size is less than 1 nm.

- A nanomaterial compound should have a surface structure in the size range between 1-100 nm.

2. Properties of nanoparticles

Nanoparticles are usually solid particles that have sole scales which make their properties exceptional and very useful in different fields [3]. These particles are known for their high stability, high reactivity and prominent optical qualities. Additionally, the

size of these nanoparticles makes them really easy to access the human body through the lungs and skin.

Consequently, these nanostructures can be dangerous when passing through the cell membranes. So, researchers are still studying the toxicity of nanoparticles and many governments are funding these kinds of studies in order to define their characteristics and toxicity effects [4].

3. Classifications of nanoparticles

Nanoparticles are usually classified based on three different standards. First being their origin (natural or anthropogenic), second being their size (1-10 nm, 10-100 nm and >100 nm) and third their chemical composition (inorganic, organic and element of the living kingdom) [5]. Mainly, the organic NPs group contains micelles, dendrimers, liposomes, compact and hybrid polymeric. On the other hand, inorganic NPs group includes quantum dots, fullerenes, silica and gold nanoparticles [6].

In fact, colloidal silica nanoparticles, also called silicon dioxide, are amorphous particles that have a spherical shape [7]. These nanostructures have emerged recently a lot in the research field due to their stability and large range of applications.

B. Mesoporous Silica Nanoparticles (MSNs)

1. Discovery of SiO_2

Silicon was discovered in 1824 by Jakob Berzelius by preparing amorphous silicon using earlier methods and then by removing fluorosilicates by washing the product and getting the purified one. The name silica comes from the Latin word *silex*. Silica is the combination of silicon atom (Si) and oxygen atom (O_2) [11].

11

Mesoporous silica was first known to the world and to scientists 40 years ago when researcher R.L. Mieville presented zeolite-silica gel mixtures that had a well-defined and uniform porosity [8]. However, this achievement almost went unnoticed until 1992 when two groups of Japanese researchers [9], [10] discovered organic-templated mesoporous silicas and researchers began to see the uniqueness of these materials.

2. Structures of silica nanoparticles

Silica is found in two different structures: crystalline and amorphous [11]. Silica is formed naturally as the solid amorphous phase of flint and opal and as the crystalline stage of cristobalite, quartz and tridymite. The amorphous form of silica can be transformed into the crystalline one by thermal treatment as shown in the equation below:

$$\text{Quartz} \xleftrightarrow{870\,^{\circ}\text{C}} \text{Tridymite} \xleftrightarrow{1470\,^{\circ}\text{C}} \text{Cristobalite} \xleftrightarrow{1710\,^{\circ}\text{C}} \text{Melting point}$$
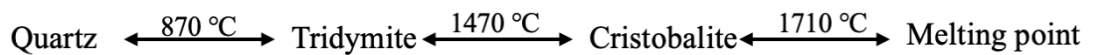
Silica has two impure forms that are quartz and sandstone.

3. Synthesis and chemistry surface

MSNs are an unusually diverse family that are synthesized mainly from one of two types of precursors that are tetraalkoxysilanes and sodium silicate solutions [12]. The most used precursor for the formation of silica nanoparticles is tetraethyl orthosilicate (TEOS) which leads to two reactions: first step is the hydrolysis of TEOS molecules that form silanol groups, and second condensation of the silanol groups

12

between each other or between them and the epoxy groups present that creates siloxane

bridges (Si-O-Si) that form the entire silica structure [13].

The general reactions of the formation of silica nanoparticles from TEOS can be

written as below [14].

$$Si(OC_2H_5)_4 + H_2O \xrightarrow{\text{hydrolysis}} Si(OC_2H_5)_3OH + C_2H_5OH$$
$$\equiv Si\text{-}O\text{-}H + H\text{-}O\text{-}Si\equiv \xrightarrow{\text{Water condensation}} \equiv Si\text{-}O\text{-}Si\equiv + H_2O$$
$$\equiv Si\text{-}OC_2H_5 + H\text{-}O\text{-}Si\equiv \xrightarrow{\text{Alcohol condensation}} \equiv Si\text{-}O\text{-}Si\equiv + C_2H_5OH$$
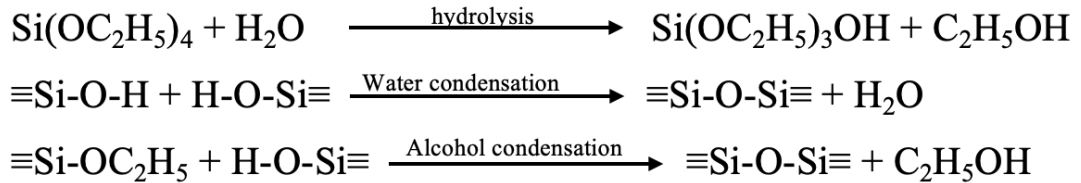
SiO_2 NPs can be synthesized based on several methods as reverse

microemulsion, flame synthesis and sol-gel method.

a. Reverse Microemulsion

The reverse microemulsion method consists of having an isotropic,

macroscopically homogeneous, and thermodynamically stable solution that contains at

least three components that are: a polar phase (typically water), a nonpolar phase

(usually oil), and a surfactant [15].

This method is easy and efficient to use especially in the formation of

nanoparticles because one can control the size of the particles by simply varying the

microemulsion parameters [16].

Lin *et al.* [17] described the formation of silica nanoparticles by reverse

microemulsion method that consisted of creating the water in oil microemulsion system

by mixing cyclohexane, CA-520 and deionized water with known quantities. Then,

TEOS and an ethanol solution of APTMS were added to the mixture. After some time,

ammonia hydroxide was added as a catalyst for the hydrolysis reaction of TEOS and

APTMS and the reaction was left to be completed at room temperature.

b. Flame synthesis

The flame synthesis method consists of oxidizing and decomposing evaporated

metal precursors in a flame, which forms stable metal-oxide monomers followed by

nucleation, aggregation or agglomeration of the aggregated nanoparticles [18]. This

method is risky due to the fact that one can't control the size or shape of the formed

particles [19].

Yue *et al.* [20] reported a one-step flame synthesis for the production of silica

nanoparticles. They used a co-flow diffusion flame burner for the synthesis of the NPs

with a diluted Argon flow in the central tube for the control of size of the final product.

HMDSO was the silica precursor, methane was the fuel and oxygen was the oxidant.

c. Sol-gel method

The sol-gel method involves the preparation of a precursor solution that turns

into a more solid-like mixture as a result of the evaporation of the solvent, dehydration,

or chemical cross-linking between solid particles or the dissolved precursor [21].

The sol-gel method is also known as the Stober's process [22] that was first

introduced in 1968 and the most common method found for the formation of silica

nanoparticles.

This method uses tetraethyl orthosilicate (TEOS) as a silica precursor that

undergoes hydrolysis in the presence of ethanol and ammonium hydroxide which later

on undertakes a polycondensation reaction to form non-porous silica nanoparticles that have a size less than 200 nm.

Also, Rao *et al.* [23] in 2005 reported a new method for the synthesis of silica nanoparticles that consisted of a sequential addition method by a sol-gel process. Their method consisted of adding 5 mL of ethanol and 5 mL of water and keeping them in a sonication bath for 10 minutes. After that, known volumes of TEOS were added while sonicating and after 20 minutes 28% ammonium hydroxide was added as a catalyst. The mixture was left in the sonication bath for 60 minutes and at the end a white turbid suspension was obtained. We should note that this method was conducted at room temperature.

Furthermore, a modified Stober's process is found to be widely used for the synthesis of MSN with a range of pore sizes going from 2 to 50 nm and that consists of incorporating cetyltrimethylammonium bromide (CTAB) that is a surfactant and site-directing agents like the triblock copolymer (F127) [24].

4. *Properties of silica nanoparticles*

In general, SiO_2 NPs are found in the form of a white powder and have a size range of 10-500 nm; the size can be controlled by varying the reaction parameters such as the concentration of ammonium/sodium hydroxide, the concentration and addition rate of TEOS and the mixing speed.

Silica nanoparticles (SiO_2 NPs) have gained so much attention in the drug delivery field because they are biocompatible, easy to synthesis, can undergo surface modification and are small in size. Mesoporous silica has a large number of empty

pores than can encapsulate large amounts of drugs. Like their size, their shape plays a major role in the biomedical applications and payload activity.

For example, Zhao *et al.* [25] synthesized three different shaped fluorescent mesoporous silica nanoparticles and compared there *in vivo* biological behavior. The three shapes synthesized were long rod nanoparticles (NLR), short rod nanoparticles (NSR) and spherical nanoparticles (NS).

All three shapes were first functionalized with carboxylic acid to obtain (SiO_2-COOH) that is capable of covalently combining to Cy5.5-hydrazide thus making them fluorescent. The results of *in vivo* showed that NLR resided longer, took more time to be cleared renally and had more extended blood circulation than NSR and NS. On the other hand, the results of *in vitro* showed that NSR were degraded faster than NS and NLR because of their high surface area.

Moreover, their surface area and pore volume could be easily controlled by varying the synthesis method parameters and also played a stronger part in their payload delivery. Generally, the pore size of SiO_2 NPs can be controlled to be between 2 and 50 nm by varying the reaction parameters [26].

For example, Li *et al.* [27] studied the effect of pore sizes of MSNs loaded with doxorubicin on anticancer efficacies. They synthesized three different MSNs with three pore sizes using the microemulsion method: MSN2 with a pore size of 2.3 nm, MSN5 with a pore size of 5.4 nm and MSN8 with a pore size of 8.2 nm. The results showed that MSN2 had the smallest loading capability (8.2%) and MSN5 presented the greatest release profile and cellular acceptance.

Furthermore, SiO_2 NPs are highly sensitive and selective towards chemical and biological analytes. Their sensing ability is defined by an electrostatic interaction

happening between the positively charged species and negative charged surface of these nanoparticles [28].

The main two advantages of these nanostructures are their capability of having different size ranges and chemistry surfaces in addition to their large surface area and stability which makes them applicable in many domains.

5. *Applications of silica nanoparticles*

SiO_2 NPs can be used as an additive for the production of rubber and plastic [29] and as strengthening filler for concrete and other construction composites [30]. On the other hand, SiO_2 NPs are used as a stable non-toxic platform for biomedical applications like drug delivery and theranostics, as adsorbents for many compounds such as organic dyes, as nanosensors for the detection of specific analytes and as catalysts for many reactions.

a. Drug delivery

The idea of using silica nanoparticles as drug carriers was first discussed in 1998 when Muller, Reck and Roser [31] filed a patent declaring that mesoporous silicates could include pharmacologically active substances, and this was considered again in 1999 by Schuth and colleagues [32].

The first paper published about MSNs releasing a drug molecule was in 2001 by Balkus *et al.* [33] and they used a material known as Dallas Amorphous Material-1 (DAM-1).

This new achievement combined with the discovery of an altered Stober's process [34] that could yield mesoporous silica nanoparticles of unchanging size and

morphology encouraged researchers in using MSNs more in the drug delivery field which thrived in today's literature.

b. Anti-bacterial agent

SiO_2 NPs can be loaded with several antimicrobials like antibiotics, peptides, and other functional materials covalently or non-covalently [26].

This covalent conjugation of antimicrobials onto the surface of the silica nanoparticles includes the usage of linker molecules like PEG crosslinkers and silane-coupling agents.

Many researchers have successfully loaded silica nanoparticles with antimicrobials and used them as carriers for the treatment of many bacteria.

For example, Gonzalez *et al.* [35] synthesized mesoporous silica nanoparticles that acted as a carrier for antimicrobial agent (levofloxacin, LEVO) that was located inside the pores. A polycationic dendrimer called the poly(propyleneimine) dendrimer of third generation (G3) was grafted covalently onto the external surface of the LEVO loaded nanoparticles to offer the nanosystem of bacterial membrane interaction ability. This nanosystem penetrated efficiently the cellular membrane of *E. coli.*

Moreover, Kavruk and co-workers [36] designed an aptamer-gated vancomycin-loaded MSN. The aptamers were specific to antigens that were present on the surface of *S. aureus* bacteria and the release of vancomycin was controlled when interaction between the aptamers and the bacterial surface happened; making this MSN efficient and highly selective.

c. Anti-cancer activity

Moreover, Si NPs have been used widely in anti-cancer treatments because their pore and particle size can be finely varied in a range of 2-50 nm and from 10 nm to micron respectively [37]. Several biomedical studies have used silica nanoparticles as anti-cancer agents.

For example, Brezaniova *et al.* [38] prepared non-porous and mesoporous silica nanoparticles modified with temoporfin by the evaporation method and studied their efficiency in breast cancer treatment. They synthesized four types of silica-based nanoformulations that were: mesoporous silica nanoparticles nonmodified (SiNP-1), modified with phenyl (SiNP-2) and 3-aminopropyl (SiNP-4) groups. They successfully developed a drug delivery system for photodynamic therapy that was based on silica NPs with temoporfin that was able to pass through the blood-brain barrier. This shows great potential to cure metastases behind blood-brain barrier.

On the other hand, Chaudhary *et al.* [39] synthesized uniformly sized (~ 60 nm) mesoporous silica nanoparticles. These NPs were modified into phosphonate MSNs (negatively charged) and amine MSNs (positively charged) and were then loaded with resveratrol (RES). They studied the effect of surface functionalization on the loading, *in vitro* discharge, anti-proliferative and cytotoxic potential of RES using prostate cancer cells. Their results showed that at a pH = 7.4, free and NH_2-MSNs loaded with RES released about 90% of the drug in the first 12 hours and PO_3-MSNs released slowly the drug with approximately 50% of it the first 12 hours. Also, at a pH = 5.5 PO_3-MSNs and NH_2-MSNs had a more controllable release with 40% less release.

d. Adsorption activity

Furthermore, SiO$_2$ nanoparticles have shown great interest recently as adsorbents for the removal of organic dyes from water due to the presence of silanol groups on the surface on these nanostructures that enable them to complex the dyes. In addition to: the easiness of grafting additional functionalities that improve the complexation process, the probability of photocatalyst grafting for the degradation of the dyes and their high chemical stability [40].

For example, Raj *et al.* [41] prepared porous silica nanoparticles (PSN) that were coated with cetyl trimethyl ammonium bromide (CTAB) using a top down approach with high temperature calcination. Three cases of PSN were prepared where the temperature of calcination was 100 ºC, 250 ºC and 500 ºC. Later on, these three PSN cases were used for the adsorption of organic dyes that included methylene blue (MB), methyl orange (MO), rhodamine B (RB) and bromo cresol green (BCG) and examined by UV-vis spectrometry. The equilibrium concentration (Q$_e$) was found to be: 295.05 mg/L for MO on adsorbent PSN-100 and 297.54 mg/L for BCG on adsorbent PSN-100 ; 271 mg/L for MO, 272 mg/L for BCG, 274 mg/L for RB and 277 mg/L for MB on adsorbent PSN-250; 286 mg/L for RB and 290 mg/L for MB on adsorbent PSN-500.

Also, Qin *et al.* [42] prepared mesoporous silica nanoparticles that had a large surface area (~ 585 m^2/g), uniform particle size (~ 30 nm), large pore volume (1.175 cm^3/g) and a narrow pore size distribution (1.68 nm) by a facile one-pot method. These NPs showed high efficacy in the adsorption process of cationic dyes that included rhodamine B, methylene blue, methyl violet, malachite green, and basic fuchsin. The maximum adsorption capacities were found to be in the range of 14.70 mg/g to 34.23 mg/g that could be achieved within 2-6 minutes using UV-vis spectrometry.

e. <u>Catalytic activity</u>

As mentioned earlier, the size and pore size of Si NPs can be modified by varying the synthesis parameters. The modifications that could be made to the pore size of these NPs have led them to be useful materials in the catalytic field [43].

In fact, Dickschat *et al.* [44] prepared bifunctional mesoporous silica nanoparticles bearing Pd complexes and other basic sites and were found to be cooperative active catalysts in the Tsuji-Trost allylation of ethyl acetoacetate. The formed MSN were prepared by co-condensation of TEOS and triethoxysilanes containing azides and alkoxyamines at their termini. The results showed that the amino functionalities present on the surface on the nanoparticles played the major role in yielding 96% of the product wanted in this reaction.

Moreover, Yang *et al.* [45] prepared a bimetallic catalyst that was based on palladium (Pd) and gold (Au) and had mesoporous silica nanoparticles (MSN) as support. This catalyst was prepared by an organic impregnation-hydrogen reduction approach. This catalyst was then put to test in order to see if it can improve the speed of the hydrogenation reaction of cinnamaldehyde (CALD). Results showed that the conversion of CALD to HALD reached its peak of 100% when the temperature increased from 25 to 100 ºC and with the presence of PdAu/MSN catalyst. Furthermore, the temperature influenced the selectivity where it was found that at 60 ºC the selectivity was 92% for HALD in the presence of PdAu/MSN.

f. <u>Sensing application</u>

Silica nanoparticles have possessed many properties that made them highly interesting and promising in the field of bioimaging and biosensing [46]. They are

capable of easily biodegrading into renal clearable molecules (i.e. silicic acid) and defecate outside the body without leaving any toxic molecules after them [47] in addition to their size and porosity. Thus, they have emerged lately as efficient sensors for many analytes and compounds.

Sung and Lo [48] published a paper in 2012 that consisted of preparing a fiber-optic sensor that was based on monodispersed hydrophobic CdSe/ZnS nanoparticles encapsulated within a silica shell and immobilized on an optical fiber by a polyvinyl alcohol (PVA) coating. The silica coated CdSe/ZnS nanoparticles were synthesized based on a micro-emulsion technique. These nanoparticles were tested for sensing Cu^{2+} ion based on the fluorescent intensity of these NPs in the presence of the ion. Results showed that the PL emission intensity of the NPs decreased linearly as the concentration of Cu^{2+} increased. The Stern-Volmer equation showed a linear response in the range of 0-10 µM with a correlation coefficient of $R^2 = 0.9858$.

On the other hand, Tan *et al.* [49] reported functionalized mesoporous silica nanoparticles (MSNPs) for the detection of H_2O_2, selective drug release and treatment against heart failure. This sensor was made of a boronic ester-based fluorescence probe that is H_2O_2 sensitive and that was attached to a surface of MSNPs that were loaded with captopril, a curative drug for heart failure, in their pores and engaged by the binding of α-cyclodextrin to the probe. When H_2O_2 was present in the tissue, it was able to react with the probe and allow the detachment of α-cyclodextrin that was present on the surface of the MSNPs and captopril could be effectively released accompanied by "turn on" of probe fluorescence.

Results showed that the detection limit of the MSNPs with the fluorescent probe towards H_2O_2 was 3.3 µM. Also, when 5 mM of H_2O_2 were added to the MSNPS sensor

the researchers observed a 1.5-fold increase in the released quantity of captopril while comparing it to the sample that had no amount of hydrogen peroxide.

g. Imaging application

Dye-doped nanoparticles have shown lots of interest for bioimaging in the recent years due to their several advantages: their capability of containing many fluorescent molecules that improves the detection sensitivity, their structure that enables the encapsulation of dye molecules in the particle matrix which shelters them from photobleaching [50]. On the other hand, MSNs have shown many interests in the imaging field due to them being mesoporous, having a large surface area and a large pore volume in addition to having a controllable particle size [51].

Santra *et al.* [52] reported in 2005 the synthesis of fluorescent, radio-opaque and paramagnetic silica nanoparticles used for bioimaging applications. The nanoparticles were synthesized using a water-in-oil microemulsion technique that consisted of Triton X-100 that is an amphiphilic molecule used as a surfactant, cyclohexane that is an oil, n-hexanol used as the cosurfactant and water. Later on, Ru(bpy) were doped inside of the silica.

The inner shell of the nanoparticles was designed to capture paramagnetic gadolinium (Gd^{3+}) ions using n-(trimethoxysilyl-propyl)ethyldiamine triacetic acid trisodium salt (TSPETE) as a silane reagent. The NPs generated MR contrast on both longitudinal (T_1) and transverse (T_2) proton relaxation times-weighted sequences. Proton T_1 and T_2 relaxativities (R_1, R_2) were calculated by measuring the change in T_1 and T_2 at increasing concentrations of NPs in distilled water using progressive saturation and multiple spin-echo imaging sequences.

Results of MR showed that Gd^{3+} ions that were linked to the nanoparticles resulted in image contrast on both T_1- and T_2-weighted images much more than using a common MR contrast agent. R_2 had a much greater value than R_1 so it's concluded that this probe will work best as a T_2 contrast agent in vivo.

C. Aims

After presenting the information related to nanoparticles and silica nanoparticles, we will focus in our work on the synthesis of silica nanoparticles.

1. The formation of silica nanoparticles is performed based on a simple synthesis route by sol-gel method. In Chapter III, we will emphasize the mechanism of the synthesis in addition to the optimization of the reaction parameters, in order to obtain the most stable and smallest in size silica nanoparticles. The reaction parameters that are optimized are as follows: the effect of silica precursor and the effect of NaOH concentration.

2. SiO_2 NPs were found to be promising material in the bioimaging and sensing domain. In recent years, there has been an increase in the presence of Ag^+ in the environment because of human activities. This increase is found in drinking water and food chains consumed by humans and leads to an accumulation of this metal ion in the human body that causes cell toxicity and organ failure. For this reason, in chapter IV the formed nanoparticles will be used in the sensing of silver ions in water.

3. People are being more and more exposed to PAHs from cigarette smoke, breathing air that contains motor vehicle exhaust, and by eating grilled or charred meats. It was shown that those who were exposed to large amounts

of naphthalene, either by skin contact or from breathing it, have developed

blood and liver abnormalities. In addition, it was proven that some PAHs can

cause cancer. In Chapter V, silica nanoparticles will be elaborated as a new

complex in the removal of benzo(ghi)perylene from aqueous solution for the

first time. The adsorption study will be achieved by measuring the

absorbance of the solution within time. The thermodynamics will also be

studied at different temperatures.

CHAPTER II

MATERIALS AND METHODS

A. Materials

Acenaphthene, acetaminophen, aluminum nitrate nonahydrate (Al $(NO_3).9H_2O$), anthracene, benzo(a)anthracene, benzo(ghi)perylene, chrysene, coronene, fluoranthene, lead (II) nitrate (Pb $(NO_3)_2$), mercury (II) nitrate monohydrate (Hg $(NO_3)_2. H_2O$), naphthalene, nickel (II) nitrate hexahydrate (Ni $(NO_3)_2. 6H_2O$), potassium nitrate (KNO_3), sodium nitrate ($NaNO_3$) and zinc nitrate hexahydrate ($Zn(NO_3)_2.6H_2O$) were obtained from Acros. Acenaphthylene, acetone, (3-aminopropyl) triethoxysilane (APTMS), benzo(b)fluoranthene, colloidal silica, dibenzo(ah)anthracene, ethanol, indenol(1,2,3,cd)pyrene, silica gel, silver nitrate ($AgNO_3$), sodium hydroxide, triethyl orthosilicate (TEOS) were acquired from Sigma Aldrich. Benzo(a)pyrene was purchased from Alfa aesar. All chemicals were used as received and dissolved in either double distilled water or acetone.

B. Sample preparation

The preparation of colloidal silica nanoparticles was carried out based on Rao *et al.* [23]*,* with some modifications (See Figure 1).

Figure 1 Schematic representation of the SiO$_2$ NPs synthesis.

To start with, 5 mL of double distilled water were mixed with 5 mL of pure ethanol and put in a sonication bath for 20 minutes. In a second step, 1 mL of colloidal silica was added drop by drop to the solvent mixture with a continuous sonication. Later on, 2 mL of NaOH (C= 1 mol/L) were added drop wise. Furthermore, the mixture was stirred for 1 hour at 400 rpm to ensure the formation of a turbid white precipitate. This precipitate was then isolated from the solution by centrifugation at 4000 rpm for 15 minutes. As ethanol was used in the beginning, the formed SiO$_2$ NPs were washed with DDW to get rid of the unreacted ethanol.

Finally, the solution was kept under freeze dryer for 24 hours in order to get a white dehydrated powder.

C. Instrumentation

For measuring resonance Rayleigh scattering spectrum synchronous fluorescence scan mode at a wavelength interval ($\Delta\lambda = 0$ nm) was used. Synchronous fluorescence scan was measured using Jobin-Yvon-Horiba Fluorolog III fluorometer

and the FluorEssence program. The excitation source was a 100 W Xenon lamp, and the detector used was R-928 operating at a voltage of 950 V instrument by keeping the excitation and emission slits width at 0 nm.

The X-ray diffraction (XRD) data were recorded using a Bruker d8 discover X-ray diffractometer equipped with Cu-Kα radiation (λ=1.5405Å). The monochromator used was Johansson type. The step size was 0.02 s and the scan rate was 20 s per step.

The Thermogravimetric Analysis (TGA) measurements were done using a Netzsch TGA 209 in the temperature range 0 to 1000 with an increment of 10/ minute in a N_2 atmosphere. Scanning electron microscopy (SEM) analysis was done using Tescan, Vega 3 LMU with Oxford EDX detector (Inca XmaW20). In short, SiO_2 powder was deposited on an aluminum stub and coated with carbon conductive adhesive tape.

Zeta potential and dynamic light scattering value were measured using Particulate systems, NanoPlus Zeta Potential/Nano Particle analyzer.

The absorption spectra were recorded at room temperature using a JASCO V-570 UV-VIS-NIR spectrophotometer in the wavelength range of 300−700 nm in a 3 mL cuvette.

N_2 adsorption−desorption isotherms were measured using a Quantachrome-NOVA 2200e-surface area and pore size analyzer.

D. Optimization of the reaction parameters

Different sizes and shapes of silica nanoparticles can be obtained when varying the reaction parameters. For this reason, various alterations were made during the

synthesis in order to study their effect on the produced NPs. The parameters that were modified are:

a)   Effect of silica precursor

b)   Concentration of NaOH

The synthesized nanoparticles were characterized using spectroscopic and microscopic techniques to check the difference between the obtained shape and size.

E. Application of Silica Nanoparticles

Silica nanoparticles have had a big importance in various fields. They have been used in drug delivery, in bioimaging, in sensing, and in many other applications. In our research work, different applications were carried out to study the efficiency and aptness of these nanoparticles. Amid those applications, we focused on:

a)   The use of SiO_2 as sensors.

b)   The efficiency of SiO_2 NPs as adsorbents for PAHs.

It is important to note that for each application, the sample preparation is developed in its specific chapter.

CHAPTER III

CHARACTERIZATION AND OPTIMIZATION OF THE REACTION PARAMETERS IN THE SYNTHESIS OF SILICA NANOPARTICLES

A. Introduction

Nanoparticles are found in many structures, having different shapes and sizes. They have various crystallinity and stability which widens their application domains [53]. There are many types of nanoparticles that are divided into two essential groups: organic and inorganic nanoparticles. Mainly the drug delivery field relies heavily on the organic nanoparticles. On the other hand, inorganic nanoparticles contain metal and metal oxide-based NPs such as silica and gold nanoparticles.

Silica is one of the few very abundant elements in the Earth's crust [54], that is found often as crystalline quartz constituted of SiO_4 tetrahedra arranged as periodic hexagonal 6-membered rings through siloxane bonds that form a bridge between two silicon centers [55].

Inside the biosphere, silica exhibits continuous hydration and dehydration that are pH dependent hydrolysis and condensation reactions. Upon dehydration crystalline silica becomes amorphous silica nanoparticles, microparticles or macroparticles [56]. The formation of amorphous silica from crystalline under the appropriate conditions, characterizes silica from other metal oxides which is attributable to the high elasticity of the siloxane bond [57].

The synthesis of amorphous silica nanoparticles is achieved by several methods [57]. The particle size, shape, pore size and pore surface chemistry of silica nanoparticles depend intensely on the synthesis process, silica precursor used,

concentration of the base used, and the concentration of silica used [58]. Silica

nanoparticles could be found as spheres, short rod and long rod [59].

Recently, silica nanoparticles that have a large surface area, uniform pores, big

pore volume and stable aqueous dispersion have been used in many applications like

biosensing, drug delivery and bioimaging [60],[61].

As mentioned earlier, the size, shape, pore surface and surface chemistry of

silica nanoparticles depend on the reaction aspects. For this reason, our work was based

on the development and optimization of the synthesis parameters in order to get the

most stable and efficient silica nanoparticles.

B. Methods of preparation

The size, shape, etc. depend intensely on the reaction parameters. For this

reason, the reaction parameters were optimized in order to prepare the most stable SiO_2

NPs. For this purpose, different silica precursors were used and different concentrations

of NaOH were studied.

1. *Effect of silica precursor*

In this step, 4 different solutions were prepared, each containing a different

silica precursor. The different silica precursors used were tetraethyl orthosilicate

(TEOS, V=1mL), (3-aminopropyl) triethoxysilane (APTMS, V=1mL), silica gel

(m=1.12 g) and colloidal silica (V=1mL).

Briefly, 5 mL of double distilled water were mixed with 5 mL of ethanol and left

in a sonication bath for 20 minutes. After that, 1 mL of the 4 silica precursors was

added (TEOS, APTMS, silica gel and colloidal silica) to the different samples followed by the addition of 2 mL of NaOH (C = 1 M).

2. *Effect of sodium hydroxide's concentration*

After choosing the adequate silica precursor, the effect of NaOH's concentration was elaborated. For this reason, a stock solution of NaOH (C= 6 M) was prepared by dissolving 2.4 g of NaOH in 10 mL of double distilled water.

From this stock solution, different concentrations of NaOH (50 mM, 100 mM, 500 mM, 1 M and 3 M), were added to the mixture of DDW, EtOH, and silica precursor. Then, the synthesis was continued as described above.

C. Results and discussion

The preparation of SiO_2 NPs was carried out through one simple synthesis route by sol-gel process. Hence, many shapes and sizes could be obtained when varying the reaction parameters.

For this reason, as described in Chapter II, different optimizations were established and the SiO_2 powder obtained was compared and characterized through XRD, TGA and SEM.

1. *Effect of silica precursor*

After one hour, when using APTMS and silica gel as precursors, no white precipitate was formed (See Figure 2).

Figure 2 Synthesis of SiO$_2$ NPs in the presence of APTMS and silica gel.

However, in the presence of colloidal silica and TEOS a white turbid suspension appeared. Meaning that, the reaction occurred only when colloidal silica and TEOS were used.

After the reaction was done, the precipitate was freeze dried and characterized through XRD, TGA and SEM.

Generally, according to Nallathambi *et al.* [62], the XRD diffraction pattern of silica nanoparticles powder usually shows a broad peak at $2\theta = 22°$. Similar results were obtained for both SiO$_2$ NPs prepared using TEOS and colloidal silica, confirming the amorphous nature of silica nanoparticles (See Figure 3). Although, a minor shift in the diffraction angle was observed for TEOS where $2\theta = 25°$. This main difference is due to the fact that TEOS presents a carbon chain (C$_8$H$_{20}$) which is absent in colloidal silica.
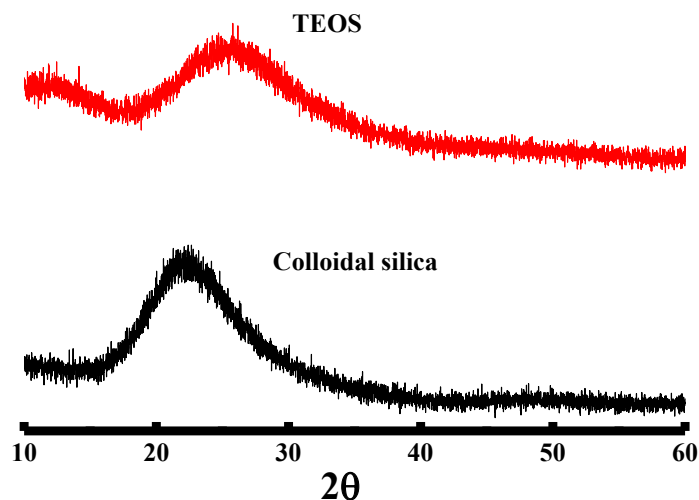
Figure 3 PXRD pattern of SiO_2 NPs prepared using colloidal silica and TEOS as silica precursor.

Furthermore, thermogravimetric analysis TGA was measured in order to check the stability of the produced NPs. As shown in Figure 4, the SiO_2 NPs were found to be highly stable with the increase of the temperature from 30 °C to 1000 °C.

The TGA analysis showed a weight loss around ~100 °C for both colloidal silica and TEOS. Initially, this weight loss is attributed to the loss of water and ethanol. Additionally, the TGA results indicate that a mass loss of ~7% happened when colloidal silica was used and of ~14% when TEOS was used. Similarly, the highest % mass loss of TEOS is mainly attributed to the presence of long carbon chain in its structure.
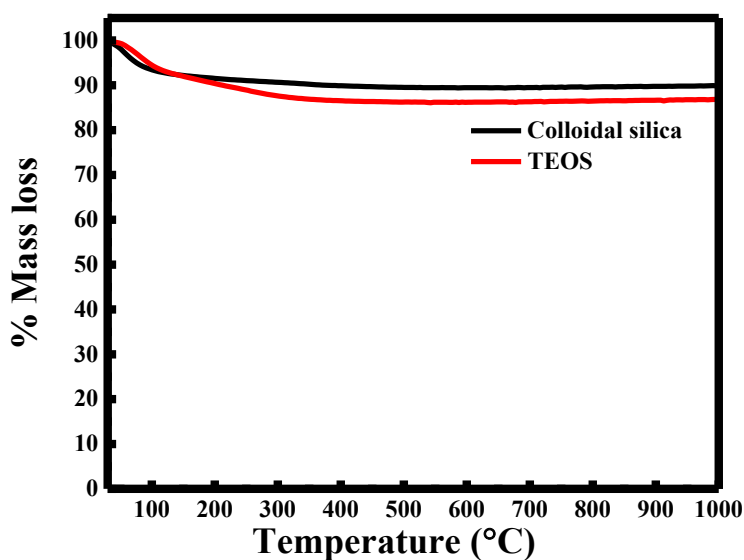
Figure 4 Thermogravimetric analysis TGA of SiO_2 NPs prepared with different silica precursors.

Finally, scanning electron microscopy SEM was carried out to compare the size of the particles obtained when varying the silica precursor. As shown in Figure 5A, when TEOS was used large spheres were obtained in the range of 300-500 μm. However, a huge difference was obtained when using colloidal silica, where the size has decreased dramatically to 40-50 nm (See Figure 5B).
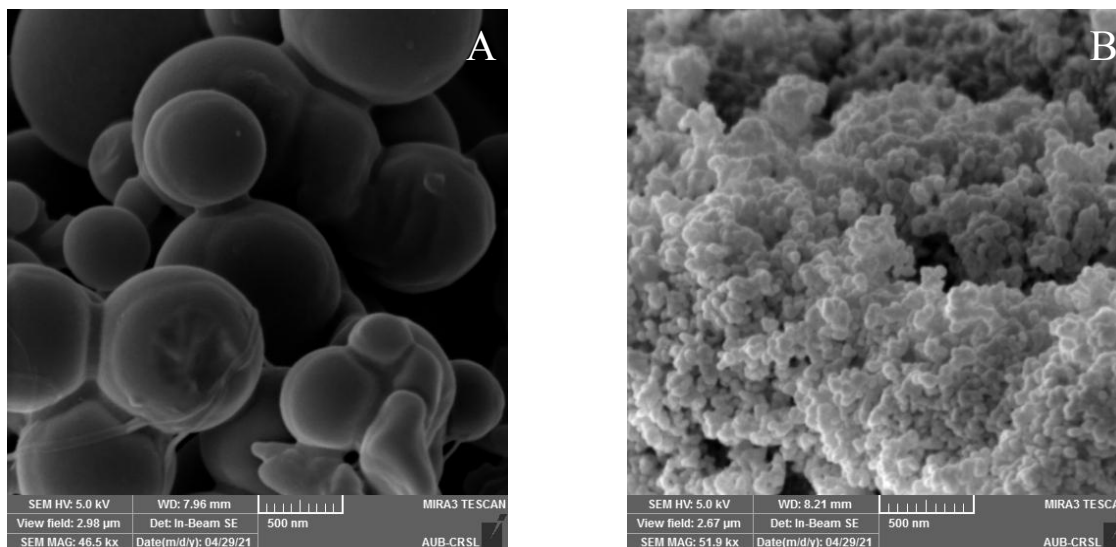
Figure 5 (A) SEM image of SiO$_2$ NPs using TEOS and (B) SEM image of SiO$_2$ NPs using colloidal silica.

To sum up, the silica precursor that will be used throughout the experiment is colloidal silica since the nanoparticles obtained using this precursor were the most stable and smallest in size.

2. *Effect of NaOH concentration*

In fact, the use of NaOH in this experiment is critical, since silicon dioxide nanoparticles are being produced. For this purpose, the concentrations of NaOH used were varied from 50 mM to 3 M and the formed NPs were compared based on the XRD, TGA and SEM.

Hence, for a concentration equal to 50 mM, the reaction was almost incomplete since after 1 hour a pale turbidity was obtained, resulting in few nanograms. However, when the concentrations were 100 mM, 500 mM, 1 M and 3 M a white precipitate appeared, verifying the total formation of SiO$_2$ NPs.

Starting with the XRD analysis, no change was found in the X-ray diffractogram of these powders. However, this was expected since the NaOH concentration has no

direct effect on the crystallinity degree of the nanoparticles. Hence a broad peak was shown at $2\theta = 22°$ meaning that no alterations were done on the amorphousness structure of these NPs (See Figure 6).
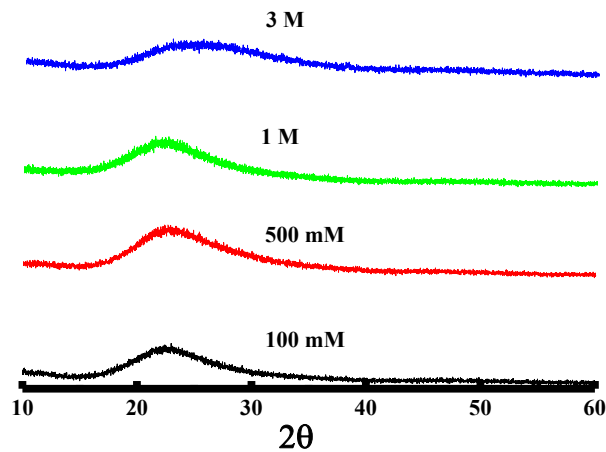
Figure 6 PXRD pattern of SiO_2 NPs prepared with different NaOH concentrations.

Moving forward to the TGA analysis, the weight loss was around ~100 ºC- 120 ºC for all the concentrations used (See Figure 7). The results indicate that the highest mass loss of ~14% happened when 3 M of NaOH were used and the lowest mass loss of ~4% occurred when 100 mM of NaOH were used. The highest % of weight loss is attributed to the weakening effect that NaOH has, at high concentrations, on the structure of the silica nanoparticles thus leading to it being unstable and degrading.
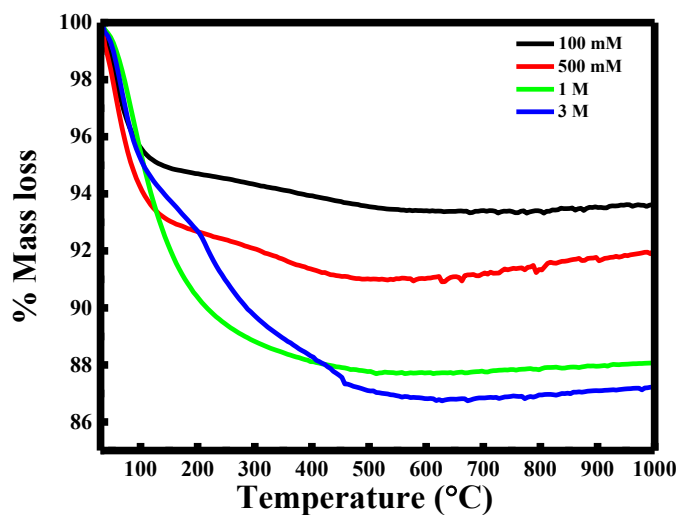
Figure 7 Thermogravimetric analysis TGA of SiO_2 NPs prepared with different concentrations of NaOH.

Finally, SEM was carried out to compare the size of NPs formed when varying the concentration of NaOH. As shown in Figure 8A-D, when the concentration of NaOH increased, the size of the NPs increased as well.

Hence, as shown visually from the SEM images the size of the formed SiO_2 NPs increased when the NaOH concentration increased from 100 mM to 3M. These results were expected, where the excess of NaOH improve the formation of aggregate in the solution.
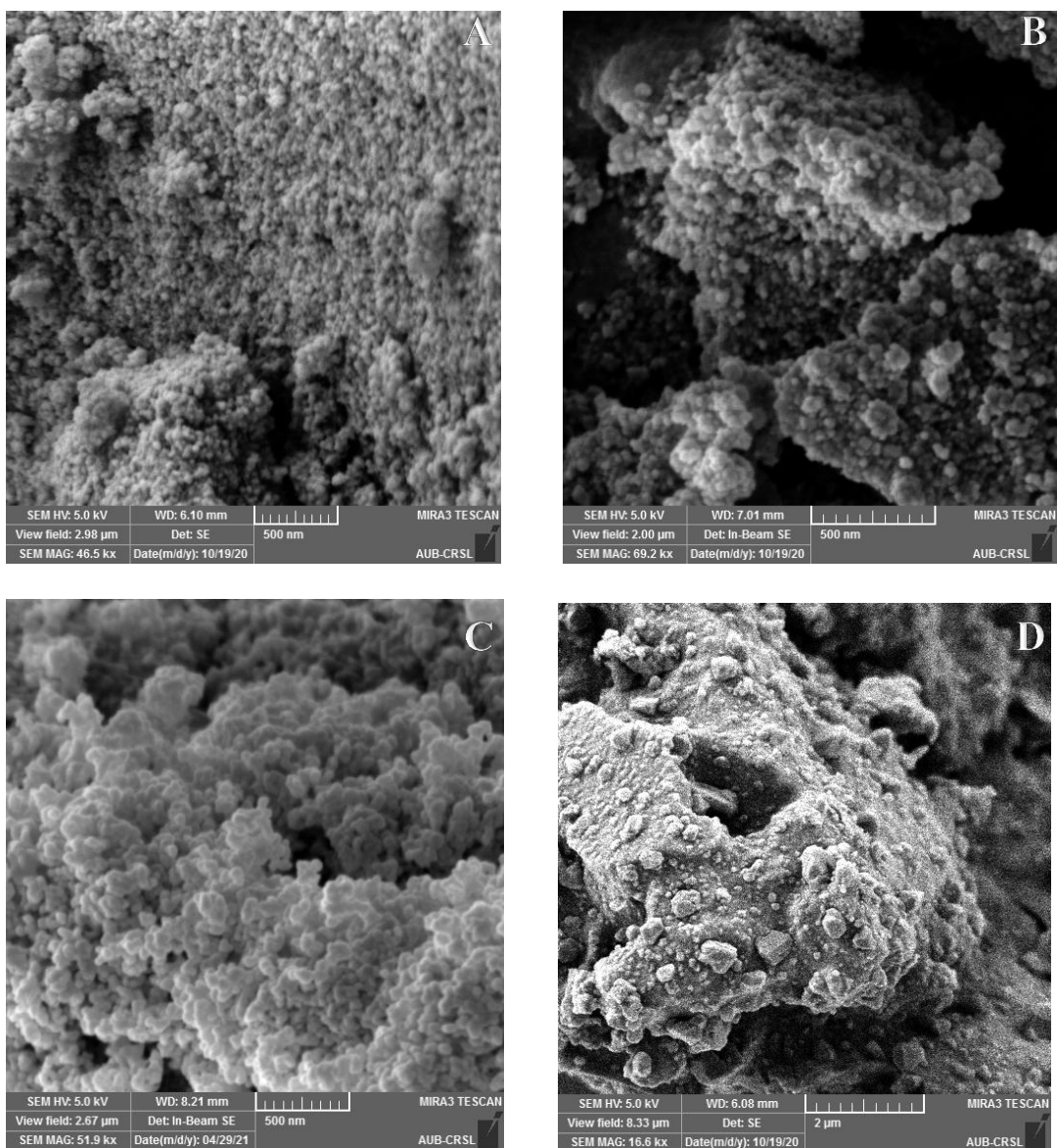
Figure 8 SEM images of SiO₂ NPs prepared with different concentrations of NaOH: (A) 100 mM, (B) 500 mM, (C) 1 M and (D) 3 M.

The concentration of NaOH that will be used throughout the experiments is 100 mM since the most stable and smallest NPs in size formed were when using this concentration.

To make sure that the synthesized silica nanoparticles were in fact SiO_2 NPs, EDX was made and illustrated below (See Figure 9).
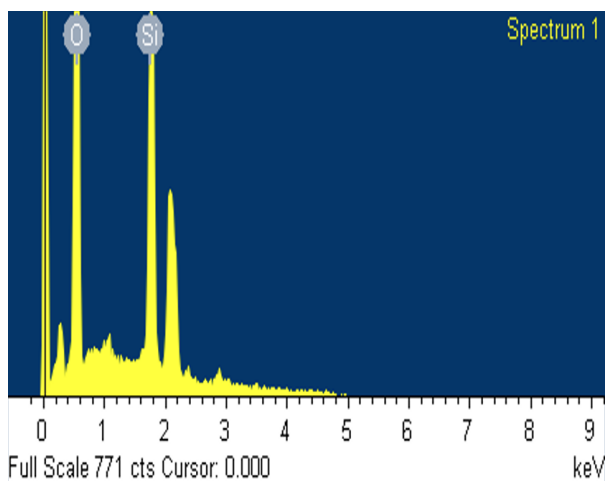
Figure 9 EDX spectrum analysis of silica nanoparticles.

As shown in the EDX spectrum, the atoms present in the sample of synthesized silica are Si and O with a % weight of 47.86 and 52.14 respectively. This indicates that the ratio of Si to O atoms is 1:2 meaning that we have SiO_2 NPs.

Finally, surface area analysis (BET) was carried out on the sample of silica in order to see its surface area value and pore volume (See figure 10).
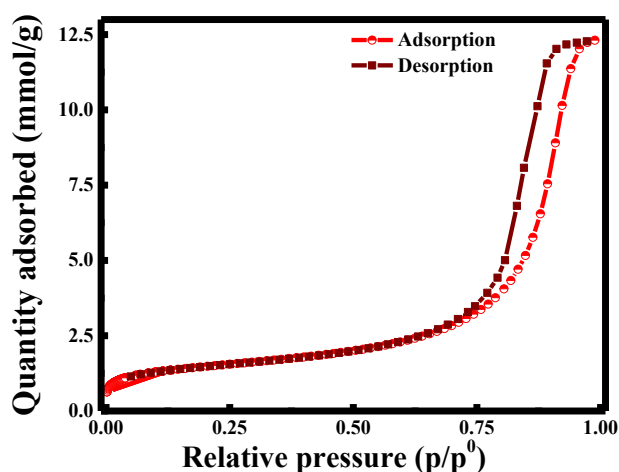
Figure 10 BET adsorption desorption isotherms for SiO_2 NPs.

BET results showed that the surface area of the synthesized silica nanoparticles was equal to 111.9291 m^2/g. Also, these results showed the pore volume of the SiO_2 NPs being less than 205.641 Å (~20.56 nm) and 2 < 20.56< 50 nm which indicates that the silica nanoparticles are mesoporous.

D. Conclusion

In conclusion, silica NPs were synthesized through a simple method by sol-gel process. It was found that the most stable and smallest NPs were formed when 1 mL of colloidal silica (0.66 M) was used in the presence of 2 mL of NaOH with a concentration of 100 mM.

CHAPTER IV

SILICA NANOPARTICLES FOR SENSING SILVER IONS USING RESONANCE RAYLEIGH SCATTERING

A. Introduction

Silver is found in the Earth's crust as its pure form and as an amalgam with gold and other metals. It's a white, soft, shiny transition metal that shows high electrical and thermal conductivity in addition to reflectivity than any other metal [63].

Silver has had many applications in various fields, such as catalysis [64], electrochemistry [65] and ant microbiology [66]. In recent years, there has been an increase in the presence of Ag^+ in the environment because of human activities. This increase is found in drinking water and food chains consumed by humans and leads to an accumulation of this metal ion in the human body that causes cell toxicity and organ failure [67]-[68]. We should note that the permissible exposure limit (PEL) set by the National Institute for Occupational Safety and Health is 0.01 mg/m^3 for all forms of silver [69].

The common methods used to detect silver ions are atomic absorption spectrometry [70]-[71], inductively coupled plasma-mass spectrometry (ICP-MS) [72]-[73], and ionic selective electrode [74]. However, these methods have many limitations due to the fact that they are expensive, require complicated sample preparations and demand experienced engineers for their repairs [75]-[76].

Lately, researchers have emerged the use of nanoparticles in the biomedical field as nanosensor for the detection of specific analytes. Hence, a sensor is by definition a device that reacts to a biological, chemical or physical pattern and interprets its reaction into a signal modification [77]. Nanosensors have arose due to many reasons like the

intense expansion of chronic diseases that cause alterations in RNAs and this necessitates advanced, cheap, fast preparation and easy recognition sensors to identify early stage illness [78].

Furthermore, to determine a perfect recognition of the irregular expression of a certain illness, the nanosensor should not interfere with the traced specific analyte. This isn't accomplished with the conventional sensors such as microelectrode or fiber optical sensors, due to their large area and size that trigger physical noise [79].

Nowadays, nanoparticles are mainly used in sensing, especially SiO_2 NPs that can sense several analytes [80] including metal ions.

For this purpose, it was in the need to find a simple, fast, with low cost technique for the detection of Ag^+ ions. Resonance Rayleigh scattering (RRS) is a method that is based upon the flexible photon scattering happening near or at photon absorption wavelengths. RRS means that for an excited sample, transmission, reflection and coherent emission in other directions exist [81]. Recently, nanoparticles in association with the RRS technique have made a great complex in the analysis of proteins. For example, Ya *et al.* [82] established an RRS test of cytochrome C using GSH capped Ag_2Te nanoparticles. It was found that the RRS intensity of the nanoprobe, that was negatively charged, improved significantly when they mixed the positively charged Cytochrome C.

In this study, SiO_2 NPs were established as nanoprobe in order to sense silver ions using resonance Rayleigh scattering technique. Finally, sensitivity and selectivity experiments will be performed.

B. Methods of preparation

1. *Sample for silver nitrate detection*

The detection of aqueous silver ions was performed using SiO_2 NPs solutions at room temperature. In summary, 500 µM stock solution of silver ions was prepared by dissolving 0.85 mg of $AgNO_3$ in 10 mL of double distilled water.

To arrange several known concentrations in the range of 0 to 500 µM a known volume of stock solution of silver ion was pipetted and added to 0.1 mg/mL of SiO_2 NPs aqueous solution. The detection of Ag^+ ions was done using resonance Rayleigh scattering.

To adjust the final concentration, a complementary volume of double distilled water was added to make a total volume of 3 mL.
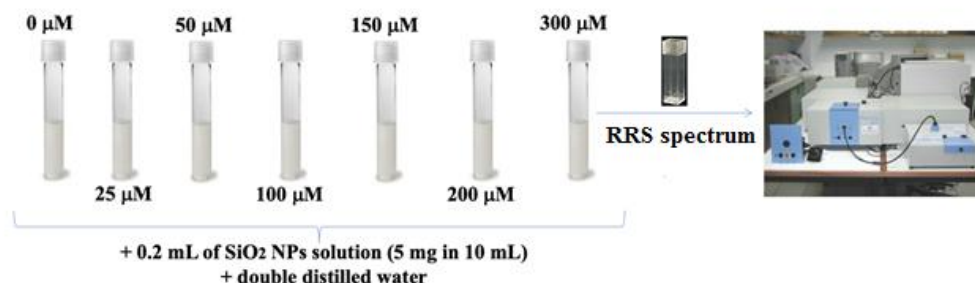
Figure 11 Scheme illustrating the preparation of $AgNO_3$ samples.

2. *Selectivity towards the nanoprobe*

The selectivity of the synthesized colloidal silica nanoparticles was investigated by using colloidal silica suspension and also by removing all silica precursors to observe the detection of silver ions.

To sum up, 1 mL of colloidal silica (~40%) was added to 9 mL DDW and used for the detection of Ag^+ as described earlier. Also, experiments were carried out where no silica was added, only silver ions and DDW.

3. Selectivity towards interference

It is of great importance to study the selectivity of a detective experiment particularly in real sample applications. Accordingly, different control experiments were done using Cu^{2+}, Hg^{2+}, Ni^{2+}, Pb^{2+}, Al^{3+}, Na^+, Zn^{2+} and K^+ to test the selectivity of our sensing approach for Ag^+ detection.

For this reason, 500 µM of each cation was used to complete the selectivity experiments.

4. Recovery of the method

To test the applicability, the proposed silicon dioxide nanoparticles were used to determine silver ions in water samples. The water samples were obtained from two different drinking water suppliers. The estimation of the analytical recovery was done on three unknown samples by using the obtained fitted calibration curves.

5. Photostability of SiO_2 NPs

Two distinctive samples were made to test the stability and to make sure that the addition of silver will not make the nanoprobe less stable throughout measurement time. In the first, 0.2 mL of SiO_2 NPs were poured into a vial and completed with double distilled water till 3 mL. In the second, the same volume of silica nanoparticles was mixed with silver nitrate and finalized with double distilled water.

These two solutions were kept undisturbed for 5 hours and then the emission intensity was measured for 1 hour in interval of 10 minutes.

C. Results and discussion

1. *Interaction between silver ions and silica nanoparticles*

Mesoporous silica nanoparticles have gained lots of interest in the biomedicine field due to their characteristics such as high surface area, large pore size, good biocompatibility and biodegradability, their stability and non-toxicity [83].

For this reason, the prepared SiO_2 NPs were used as a nanoprobe to detect silver ions. The efficiency of these nanoparticles was compared to the activity of colloidal silica precursor alone without any modifications.

The sensing of $AgNO_3$ was done for a concentration range going from 5 to 300 µM which includes the permissible exposure limit that is equal to 92.7 µM. Figure 12 shows the RRS spectra of SiO_2 after adding different concentrations of silver ions. The RRS peak of SiO_2 presented at $\lambda = 398$ nm has been proportionally improved with the increase in silver ions concentrations. This increase in the RRS intensity is due to the adsorption of Ag^+ ions onto the mesoporous surface of the SiO_2 NPs.
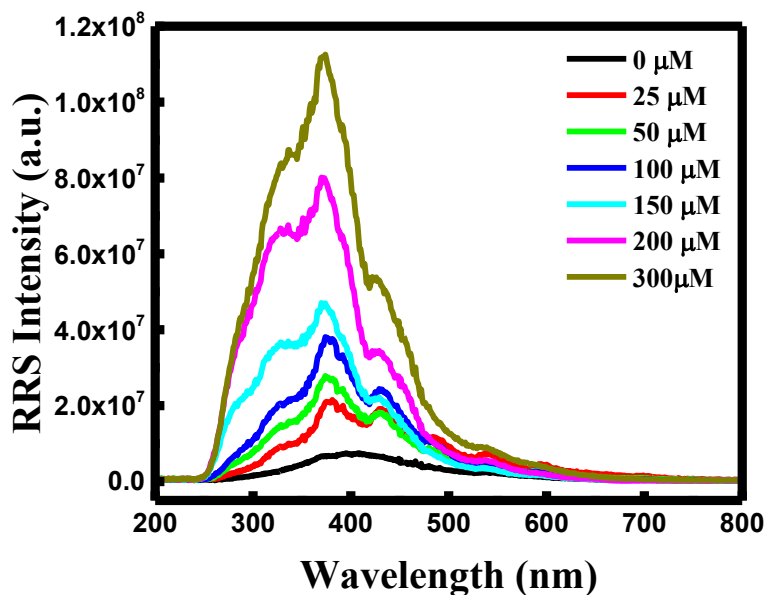
Figure 12 RRS spectrum of SiO$_2$ NPs in the presence of silver cations in the range of 5-300 μM (n=3).

As mentioned earlier, the increase in the RRS intensity was attributed to the adsorption of positively charged Ag$^+$ to the negatively charged mesoporous SiO$_2$ NPs nanoprobes. This is a result of electrostatic interaction between opposite charged species. According to Eftekhari *et al.* [84], silica nanoparticles are negatively charged in a pH range of 2 to 14. This confirms the electrostatic interaction happening between the negatively charged SiO$_2$ NPs and the Ag$^+$ ions.

This was also verified when analyzing the surface charge of the nanosensor, and the mixture. In fact, the surface charge of the SiO$_2$ NPs was equal to -19.08 mV. The charge of the surface increases to -4.28 mV upon the addition of silver ions. This change in the surface charge reveals the presence of more positive species which are related to silver ions (See Figure 13).
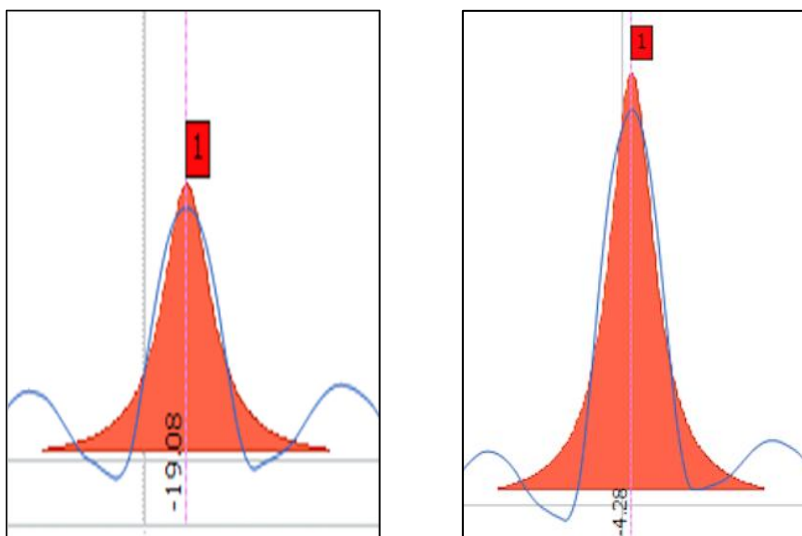
Figure 13 (A) Zeta potential value of SiO_2 NPs and (B) zeta potential value of SiO_2 NPs-Ag^+ mixture.

Furthermore, the RRS intensities at $\lambda = 398$ nm have been plotted versus the concentration of silver ions in the range 5-300 µM. Figure 14 shows a linear increase in the RRS within the increase of the concentration, with an equation $y = 339050.51x + 8.63 \times 10^6$ and regression coefficient R^2 equal to 0.9916. In addition, the limit of detection (LOD) and quantification (LOQ) were found to be 130 nM and 405 nM respectively and were calculated based on the linear fit that was the plot of the RRS intensity vs. the concentration of silver ions (See Figure 14). The slope was found to be 339050.51 and the intercept was 8.63×10^6. From the slope and intercept the LOD and LOQ values were calculated referring to $k\sigma/s$ criteria, where σ is the standard deviation of y-intercepts of regression lines, k is the constant (k=3.3 for the LOD and k=10 for LOQ), and s is the slope of the calibration curve.
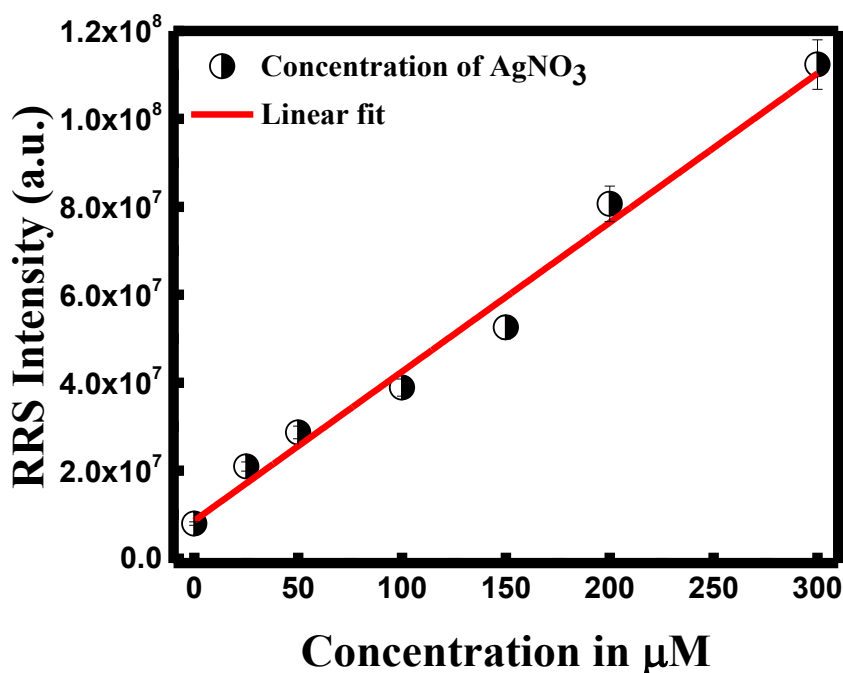
Figure 14 Linear fit of the proposed method in the range of 5-300 μM.

The obtained results reveal that our RRS method leads to a comparable linear range and limit of detection to those of previously reported methods. Several linear ranges and detection limits of different techniques used by other workers for the Ag^+ ions determination were summarized in Table 1.

Sensing technique	Range	LOD	Interference studied	Reference
Fluorescence Biosensor Based on C-Ag+-C Structure and Exonuclease III-Assisted Dual-Recycling Amplification.	5-1500 pmol/L	2 pmol/L	Na^+, Hg^{2+}, Pd^{2+}, Cd^{2+}, Cu^{2+}, Zn^{2+}, Ni^{2+}, Al^{3+}, Fe^{3+}	[85]

Technique	Linear range	LOD	Interfering ions	Ref.
Colorimetric Detection	10^{-2}-10^4 nM	80 pM	NH_4^+, Na^+, K^+, Li^+, Ba^{2+}, Ca^{2+}, Cd^{2+}, Co^{2+}, Cu^{2+}, Fe^{2+}, Mg^{2+}, Mn^{2+}, Ni^{2+}, Pb^{2+}, Zn^{2+}, Al^{3+}, Cr^{3+}, Fe^{3+}, Cu^+, Pd^{2+}, Hg^{2+}	[86]
Fluorescent detection with organic nano-aggregates.	----	11 ppb	Na^+, K^+, Cr^{3+}, Mn^{2+}, Fe^{2+}, Fe^{3+}, Hg^{2+}, Co^{2+}, Ni^{2+}, Cu^{2+}, Zn^{2+} and Pb^{2+}	[87]
Detection of silver ions using DNA based nano-porous micro-resonator	10 nM-1 pM	1 nM	Na^+, Li^+, Ca^{2+}, Mg^{2+}, Zn^{2+}, and Fe^{2+}	[88]
Colorimetric detection using Gold Nanoparticles in the Presence of Ascorbic Acid	2-28 µM	0.85 µM	Al^{3+}, Mg^{2+}, Mn^{2+}, Ni^{2+}, Ca^{2+}, Zn^{2+}, Na^+, Co^{2+}, Cu^{2+}, Cd^{2+}, Fe^{2+}, Fe^{3+}, Pb^{2+}, Hg^{2+} and K^+	[89]
RRS using silica nanoparticles	5-300 µM	130 nM	Cu^{2+}, Hg^{2+}, Ni^{2+}, Pb^{2+}, Al^{3+}, Na^+, Zn^{2+} and K^+	Our work

Table 1 Different techniques used for the detection of Silver ion.

2. *Selectivity towards nanoprobe*

Moreover, the selectivity of SiO_2 NPs towards the sensing of silver ions was established in the first place by using colloidal silica suspension and no silica precursor at all.

Figure 15 shows the ratio of the emission intensity I/I_0 when using colloidal silica and removing all silica precursors.
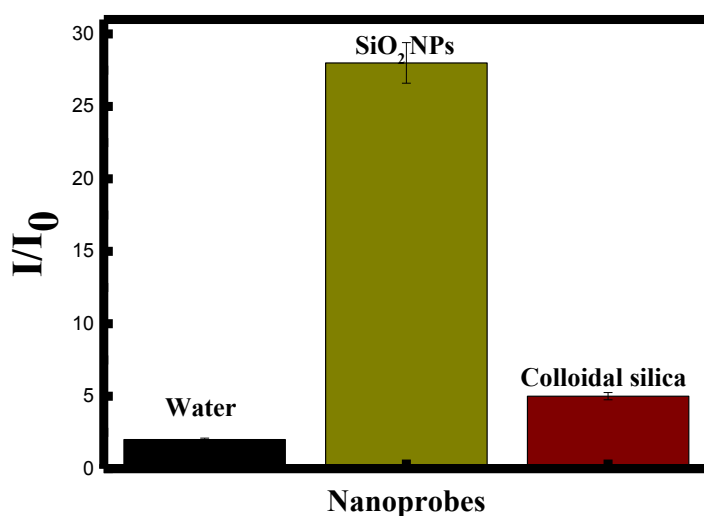
Figure 15 I/I_0 of SiO_2 NPs in the presence of different nanoprobes.

It is clear that no RRS intensity was recorded when using colloidal silica suspension and when removing all silica precursors from the solution. Thus, the enhancement of the emission intensity using SiO_2 NPs was about ~28 fold although it was ~1 fold for colloidal silica suspension and no silica at all.

These results confirm the direct interaction of negatively charged silica nanoparticles with positively charged silver ions resulting in the formation of a highly soluble complex meaning that after mixing the silver ions with the silica nanoparticles there was no precipitation at the bottom of the vial.

51

3. Selectivity towards other analytes

It is of great importance to study the selectivity of a detective experiment particularly in real sample applications. Accordingly, different control experiments were done using Cu^{2+}, Hg^{2+}, Ni^{2+}, Pb^{2+}, Al^{3+}, Na^+, Zn^{2+} and K^+ to test the selectivity of our sensing approach for Ag^+ detection.

For this reason, 500 µM of each cation was used to complete the selectivity experiments. The ratio of the RRS intensity in the presence of these analytes to the RRS intensity in the absence of these analytes (I/I_0) was measured and shown in Figure 16.
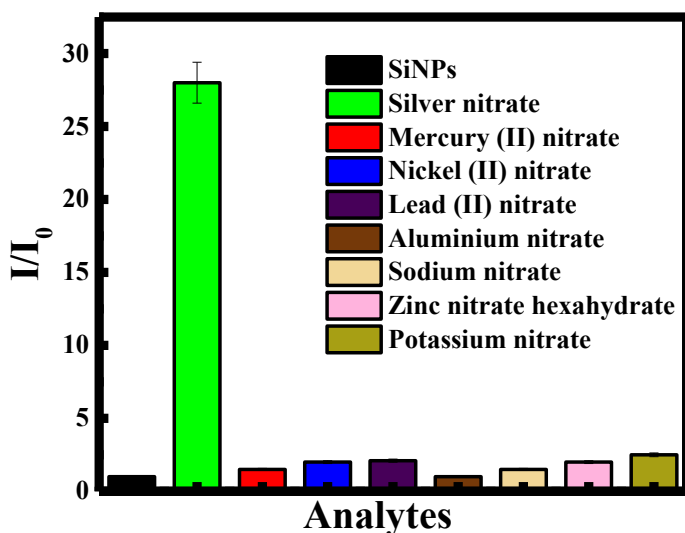
Figure 16 I/I_0 of SiO_2 NPs in the presence of 500 µM for different cations.

I/I_0 ratio showed a same value of ~2 for Ni^{2+}, Pb^{2+}, Zn^{2+} and K^+. This value decreased and reached ~1 for Hg^{2+} and Na^+ and a value of ~0.5 for Al^{3+}. However, for Ag^+, I/I_0 ratio was ~28.

Thus, it is clear that the synthesized silicon dioxide nanoparticles were extremely selective towards Ag^+ ions.

4. *Recovery of the method*

The proposed silicon dioxide nanoparticles were used to determine silver ions in water samples. The water samples were obtained from two different drinking water suppliers.

The original drinking water samples show no detectable silver ions. Then each sample had been spiked with known concentration of silver ions in order to get the recovery of the experiment. The recovery percentages of the spiked samples were in the range 98.4%-100.4% (See Table 2).

	Theoretical Concentration (µM)	Experimental concentration (µM)	Recovery (%)
Unknown 1	5	4.98	99.6
Unknown 2	75	73.8	98.4
Unknown 3	250	251.01	100.4

Table 2 Percentage recovery of the proposed method.

5. *Photostability of SiO$_2$ NPs*

The photo-stability of SiO$_2$ NPs in the presence and absence of Ag$^+$ ions is illustrated in Figure 17.

It was found that when the RRS intensity of SiO$_2$ NPs was noted in the presence and absence of Ag$^+$ for one hour, the signal was found to be stable which indicates that the current sensor is relatively stable during measurement time.
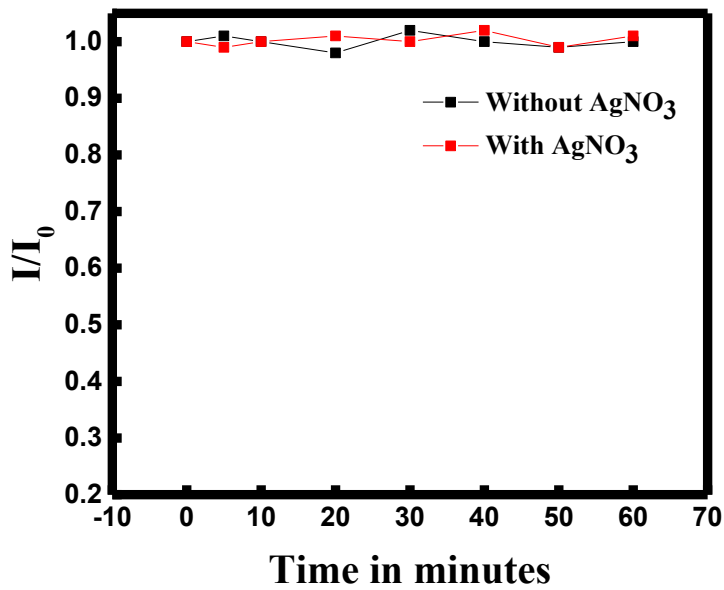
Figure 17 Plot of I/I_0 of SiO_2 NPs with time in the absence and presence of $AgNO_3$.

6. Characterization of SiO₂ after the addition of Ag⁺

EDX was done next in order to make sure that there was detection of Ag^+ on the surface of SiO_2 NPs.
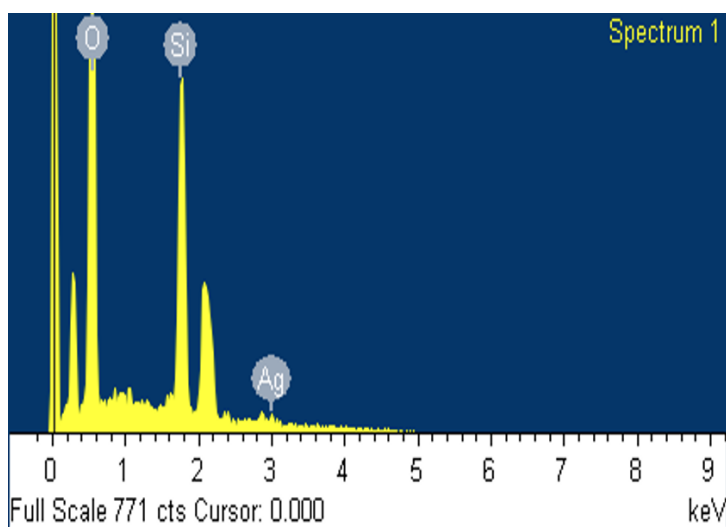
Figure 18 EDX spectrum analysis of silica nanoparticles after the addition of Ag^+.

EDX spectrum shows clearly the presence of silver ions in addition to the oxygen and silicon ones proving with that there was detection of Ag^+ on the surface on the SiO_2 NPs.

D. Conclusion

Silica nanoparticles have shown to be a great nanoprobe for the detection of silver ions in water. The synthesis of these NPs in basic media makes their surface negatively charged which encourages the electrostatic interaction between their surface and the positively charged ions.

The method used was selective and sensitive towards the detection of Ag^+ using SiO_2 NPs as nanoprobe. The recovery of the method was found to be between 98 and 100% and the limit of detection was 130 nM.

CHAPTER V

KINETICS, ISOTHERMS AND THERMODYNAMICS STUDY OF BENZO(GHI)PERYLENE ADSORPTION: SILICA NANOPARTICLES AS AN EFFICIENT ADSORBENT COMPLEX

A. Introduction

Polycyclic aromatic hydrocarbons (PAHs) are a group of chemicals that are composed of aromatic hydrocarbons that consist of only hydrogen and carbon atoms with two or more bonded benzene rings with many structural configurations [90],[91]. They don't contain hetero atoms or carry substituents in their structures [92].

PAHs are classified into two groups, light and heavy PAHs. The light PAHs are the ones that contain up to four rings and the heavy PAHs are the ones containing more than four rings [93]. Heavy PAHs are more stable and more toxic than the light ones [94].

Generally, when the size of a PAH increases its hydrophobicity and electrochemical stability increase as well [95]. This increase in hydrophobicity and stability makes a PAH more persistent in the environment.

The major way of human exposure to PAHs is from breathing air that contains them such as indoor fireplaces and car exhaust, eating food burnt or well-cooked and smoking cigarettes [96].

Continuous exposure to PAHs can cause eye irritation, nausea, vomiting and diarrhea. Excessive exposure to mixtures of PAHs, especially workers in the industry field or automobile industry, has shown to cause cancer [97]. The most common PAHs

that have been studied are: naphthalene, fluorene, anthracene, phenanthrene, fluoranthene, benzo(a)anthracene, pyrene, benzo(a)pyrene, benzo(b)fluoranthene, dibenzo(a,c)anthracene, benzo(ghi)perylene and coronene [98].

PAHs in air, water, food, soil and waste sludge are removed using the suitable organic solvent before putting them in the analytical or separating equipment [99],[100]. The common analytical method used are GC, high performance thin layer chromatography (HPTLC) and Fourier transform infrared spectroscopy (FTIR) [101].

However, Zhao *et al.* [102] determined PAHs in environmental water using magnetite nanoparticles.

Benzo(ghi)perylene is a six-ring aromatic hydrocarbon that has a molecular weight of 276.3307 g/mol and is produced by incomplete combustion of organic compounds [103]. It is the chief constituent of PAHs that is measured by the United States Environmental Protection Agency [104],[105]. It is found in some urban and rural places with a concentration range between 1.46 and 1.55 ng/m^3 [106],[107]. The 1983 International Agency for Research on Cancer's first study on benzo(ghi)perylene showed that it was not carcinogenic to animals and humans hence its research has been almost stationary. However, in recent years, lots of studies showed that benzo(ghi)perylene formed adducts with DNA to form lung tumor, in addition to it synergizing with benzo(a)pyrene to rise carcinogenic effects [108],[109],[110].

Silica nanoparticles have had so much interest in the adsorption field due to their structural characteristics like large surface area, tunable pore volumes, high thermal and chemical stability in addition to them being able to be modified easily, selective towards organic pollutants and economically recoverable [111].

In our work, the adsorption of benzo(ghi)perylene was established and managed at different concentrations of SiO_2 NPs and different concentrations of benzo(ghi)perylene.

B. Methods of preparation

For each adsorption experiment, 5 mg of SiO_2 NPs were dispersed in 1 mL of double distilled water and sonicated for 1 minute to assure complete dissolution of SiO_2 NPs. Benzo(ghi)perylene solution (C= 500 µM) was prepared by dissolving 0.41 mg of this PAH in 3 mL acetone (See Figure 19).
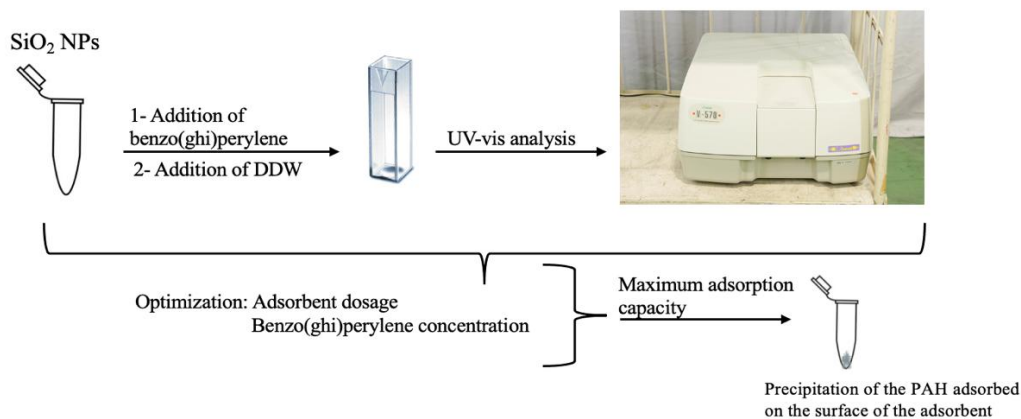
Figure 19 Scheme illustrating the preparation of adsorption sample.

In order to make sure that maximum adsorption of the PAH onto the surface of the nanoparticles is reached; the adsorbent dose and benzo(ghi)perylene concentration were varied, the pH and temperature were modified.

- In the first place, a fixed amount of benzo(ghi)perylene (25 µM, 0.15 mL) was added to different mass of SiO_2 NPs adsorbent (2-10 mg).

- In the second place, the concentration of benzo(ghi)perylene was varied from 25 to 100 μM while the adsorbent dose stayed fixed (10 mg).

- In the third place, a fixed amount of benzo(ghi)perylene (25 μM, 0.15 mL) and a fixed dose of silica (10 mg) were mixed with a complementary volume having different pHs (3,7 and 9).

- Finally, a static quantity of benzo(ghi)perylene (25 μM, 0.15 mL) was mixed with a fixed dose of silica (10 mg/mL) and the temperature was increased from 19 to 40 °C.

The total volume was kept constant and equal to 3 mL in all of these adsorption experiments. The analysis and the adsorption kinetics were monitored through UV-visible spectrophotometer at different time intervals (t=0, 5, 10, 15, 20 and 30 minutes). The sample was taken at 30 minutes, centrifuged for 2 minutes at 6000 rpm and then the absorbance was measured.

C. Results and discussion

1. Adsorption of Benzo(ghi)perylene

Generally, the shape of UV-Visible spectra of PAHs is linked to the number of aromatic rings present and their arrangement. Hence, a general bathochromic effect is observed as the number of aromatic rings increases in the PAH molecule until it reaches a maximum number of rings. Thus, the bathochromic effect of benzo(ghi)perylene is considered relatively weak since it possesses 6 aromatic rings in its structure [112].
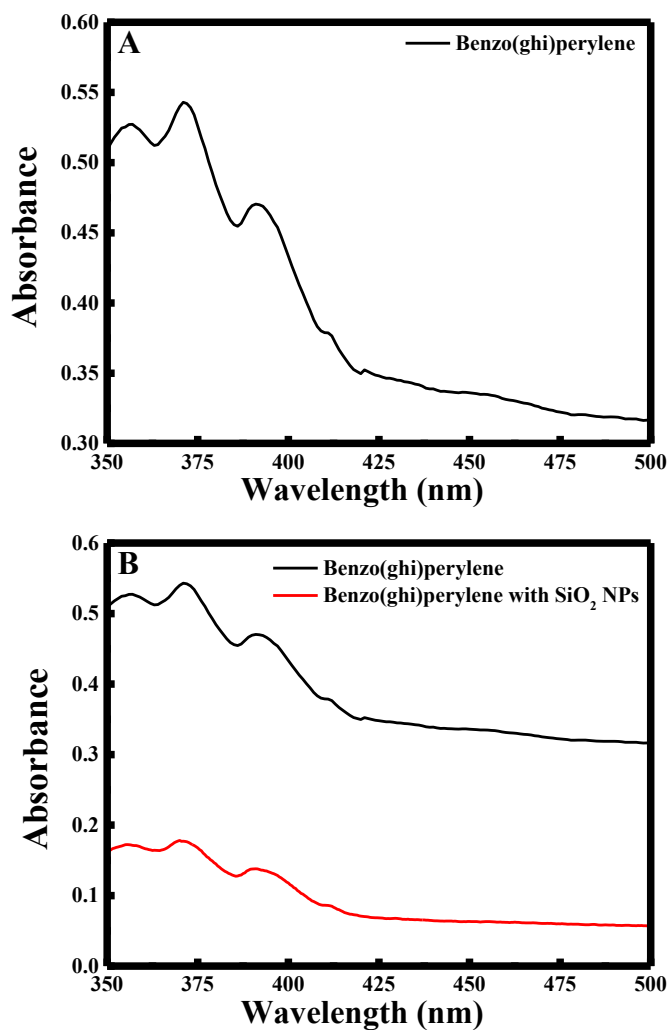
Figure 20 UV-visible spectrum of (A) benzo(ghi)perylene alone; (B) benzo(ghi)perylene with and without the addition of SiO$_2$ NPs.

As shown in Figure 20A, benzo(ghi)perylene present three major absorption wavelengths at ~354 nm, ~370 nm, and 391 nm. Remarkably, these absorption peaks were not altered after the addition of SiO$_2$ NPs meaning that there was no degradation of the adsorbate, thus it is adsorbed on the surface of SiO$_2$ NPs (See Figure 20B).

As described in section B, 1 mL of SiO$_2$ NPs were mixed with 0.15 mL (25 μM) of benzo(ghi)perylene and 1.85 mL of double distilled water, and the absorbance was measured using UV-visible spectrophotometer. Table 3 presents the variation of the absorbance of SiO$_2$ NPs with benzo(ghi)perylene within time.

Time (minutes)	Absorbance
0	0.84
5	0.56
10	0.47
15	0.44
20	0.41
30	0.23

Table 3 Variation of the absorbance of SiO_2 NPs with benzo(ghi)perylene within time.

Interestingly, the absorbance of benzo(ghi)perylene decreases with the increase in time. The adsorption capacity was calculated based on the equation below:

$$Qe = \frac{(Co - Ce)V}{m} \qquad (1)$$

where C_0 and C_e are the initial concentration and the equilibrium concentration of benzo(ghi)perylene respectively (mg/L), V is the volume of the solution (L) and m is the mass of SiO_2 NPs (g). It was found that the q_e in this case was equal to 8.49 mg/g.

2. *Optimization of the adsorption process*

The adsorption study was done at 4 initial stages: first of all, the dose of the adsorbent was optimized, secondly the concentration of benzo (ghi) perylene was varied and finally the pH and temperature of the solution were modified.

a. Effect of adsorbent dosage

The adsorption process of Benzo (ghi) perylene was studied by varying the SiO_2 NPs dosage from 2-10 mg.

In fact, increasing the amount of the adsorbent will increase the number of available adsorption sites on its surface, thus leading to an increase in the adsorption capacity.

As shown in Figure 21, the increase in the adsorbent amount improves the adsorption of benzo(ghi)perylene and enhances the adsorption capacity q_e.
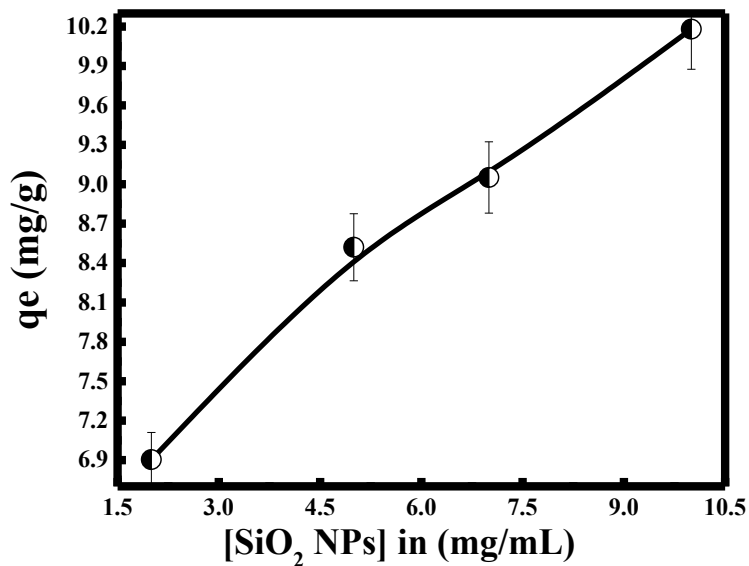
Figure 21 Variation in the adsorption capacity value q_e for different doses of SiO_2 NPs (n=3).

The adsorption capacity was found to be between 6.90 and 10.18 mg/g when varying the SiO_2 NPs dose from 2 to 10 mg. Thus, the adsorbent dose and the adsorption capacity are directly proportional with a maximum q_e equal to 10.18 mg/g when the amount of SiO_2 NPs used was equal to 10 mg/mL.

b. Effect of PAH concentration

The concentration of benzo (ghi) perylene was varied in order to determine its effect on the adsorption capacity.

At a fixed adsorbent amount of 10 mg, the PAH concentration was changed in a range of 25-100 µM. The results are depicted in Figure 22.
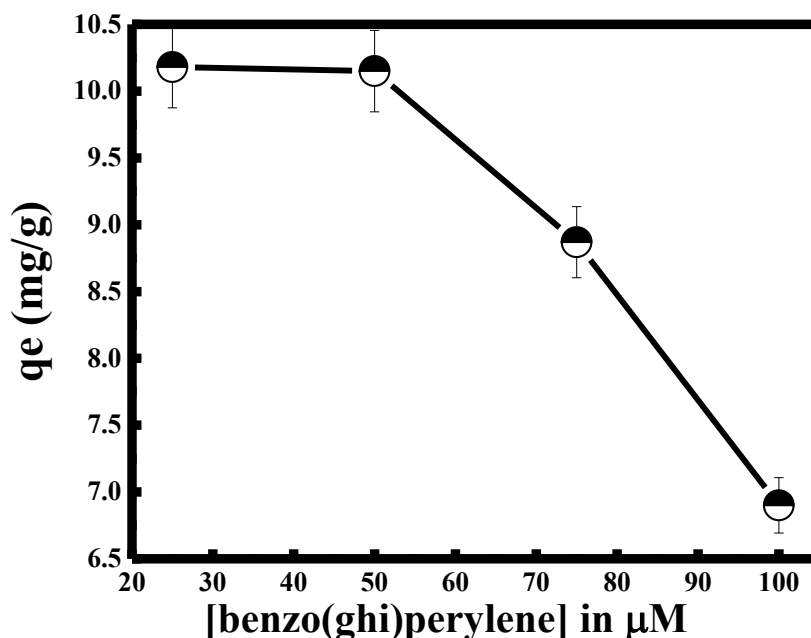
Figure 22 Variation in the adsorption capacity value q_e for different concentrations of benzo(ghi)perylene (n=3).

As expected, the adsorption capacity decreases with the increases of the PAH concentration. The adsorption capacity q_e clearly decreased from 10.18 to 6.95 mg/g when the PAH concentration increased from 25 to 100 µM. This is due to the fact that at low concentration of benzo(ghi)perylene (25 µM), the PAH compound has the ability to get adsorbed easier onto the surface of SiO_2 NPs, leading to higher adsorption capacity, until equilibrium is reached.

It is also remarkable that at high concentration of the PAH, the adsorption capacity is high enough proving the efficiency of SiO_2 NPs as adsorbent. In other words, after adsorbing a particular amount of the PAH, the adsorption sites on the surface of the adsorbent will become saturated. Accordingly, 25 µM of

benzo(ghi)perylene is completely adsorbed onto the surface of SiO$_2$ NPs, with a maximum adsorption capacity q$_e$ of 10.18 mg/g.

c. Effect of pH

In fact, pH has direct influence on wastewater treatability, regardless of whether treatment is physical/chemical or biological. Based on this, it is such a great of interest to test the pH effect on the adsorption process. Hence 3 experiments were conducted each containing 0.15 mL (25 µM) of benzo (ghi) perylene, 1 mL of SiO$_2$ NPs (10 mg/mL) and 1.85 mL of complementary volume having a different pH equal to 3, 7, and 9 respectively.

Remarkably, the adsorption capacity q$_e$ increased with the increase of pH, where the adsorption capacity q$_e$ was enhanced from 6.83 mg/g at pH = 3 to q$_e$ = 11.71 mg/g at pH = 9 (See Figure 23).
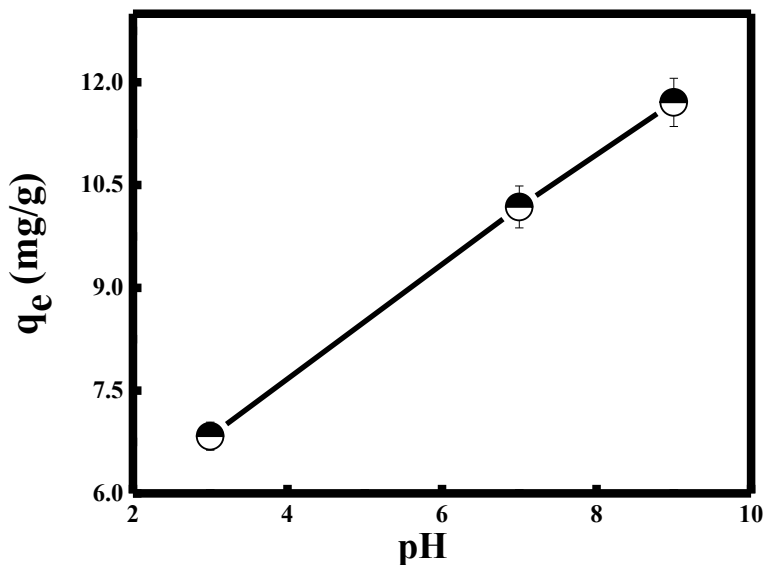
Figure 23 Variation in the adsorption capacity value q$_e$ for different pHs (n=3).

The effect of pH was analyzed by measuring the zeta potential value of SiO_2 NPs alone, benzo(ghi)perylene alone, and their mixture (See Figure 24).
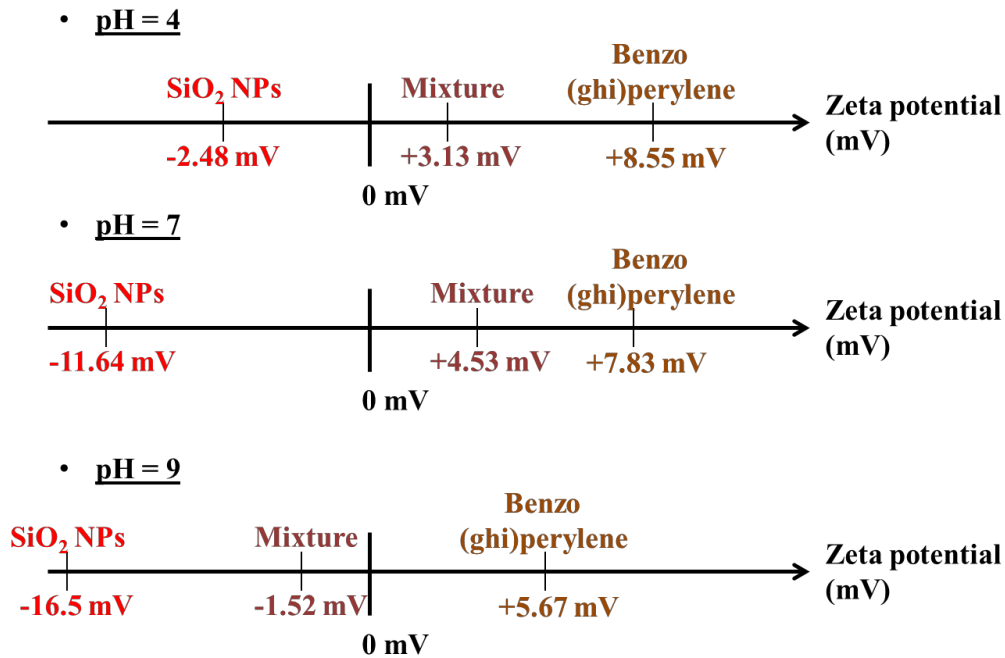
Figure 24 Zeta potential analysis for SiO_2 NPs, benzo(ghi)perylene, and the mixture at different pHs.

In fact, in neutral media SiO_2 NPs present a negatively charged surface with zeta potential value equal to -11.64 mV and benzo(ghi)perylene present a positive surface charge value that is equal to $+7.83$ mV.

Henceforth, the adsorption process reigning is an electrostatic interaction between opposite charged species. This interaction is verified by the surface charge of the mixture where it decreases to $+4.53$ mV.

Consequently, in basic medium the negativity charge of SiO_2 NPs surface will be enhanced which is explained with a zeta potential value of -16.5 mV and leading to more PAH being adsorbed onto the surface which will improve the value of q_e that is obtained.

Moreover, in acidic medium, there is a high chance that the negatively charged oxygen atoms on the surface of SiO_2 NPs bond to the hydrogen atoms (H^+) present in the solution, hence reducing the surface charge of the silica nanoparticles where the charge was equal to -2.48 mV and therefore not allowing the PAH to be adsorbed in the pores, i.e. there will be blockage of pores which explains the low value of q_e obtained at this pH.

d. Effect of temperature

Moreover, the temperature was varied to see its effect on the adsorption mechanism. Hence, 0.15 mL (25μM) of benzo (ghi) perylene were mixed with 1 mL of SiO_2 adsorbent (10 mg/mL) and 1.85 mL of double distilled water was added to this mixture.

The temperature was set at 19 °C, 25 °C, 35 °C and 40 °C and the adsorption capacity q_e was calculated respectively. Figure 25 shows the variation of q_e with the temperature.
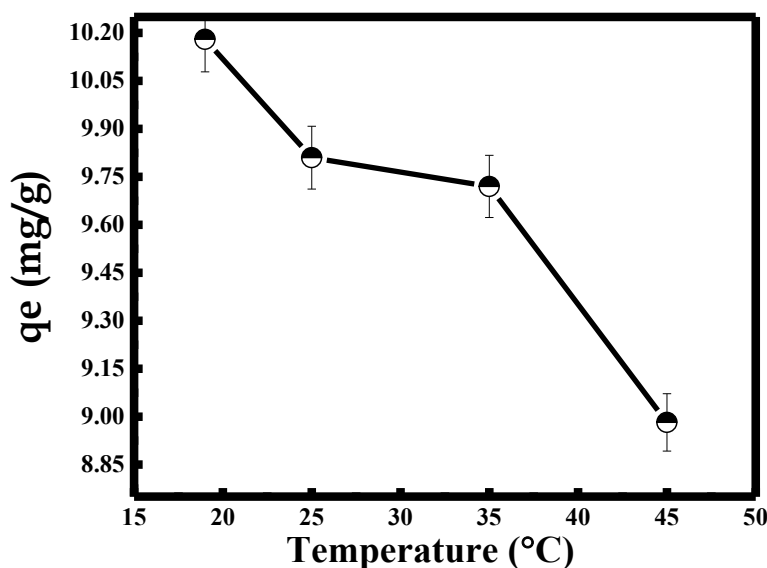
Figure 25 Variation in the adsorption capacity value q_e for different temperatures (n=3).

It is obvious from Figure 25 that the adsorption capacity decreased with the increase of temperature. Hence, q_e decreased from 10.18 and reached 8.98 mg/g when the temperature increased from 19℃ to 40℃.

This decrease of q_e with the increase of temperature shows that the adsorption process is exothermic. This may be due to the adsorptive forces between the PAH compound and the active sites on the adsorbent's surface that decreases with the increase of temperature [113].

3. *Kinetic study*

The adsorption kinetics of benzo(ghi)perylene onto the surface of SiO_2 NPs was established at a benzo (ghi) perylene concentration of 25 μM and adsorbent dose of 10 mg.

The kinetics studies of the adsorption process for the pseudo-first and pseudo-second orders are shown in Figure 26 A&B respectively.
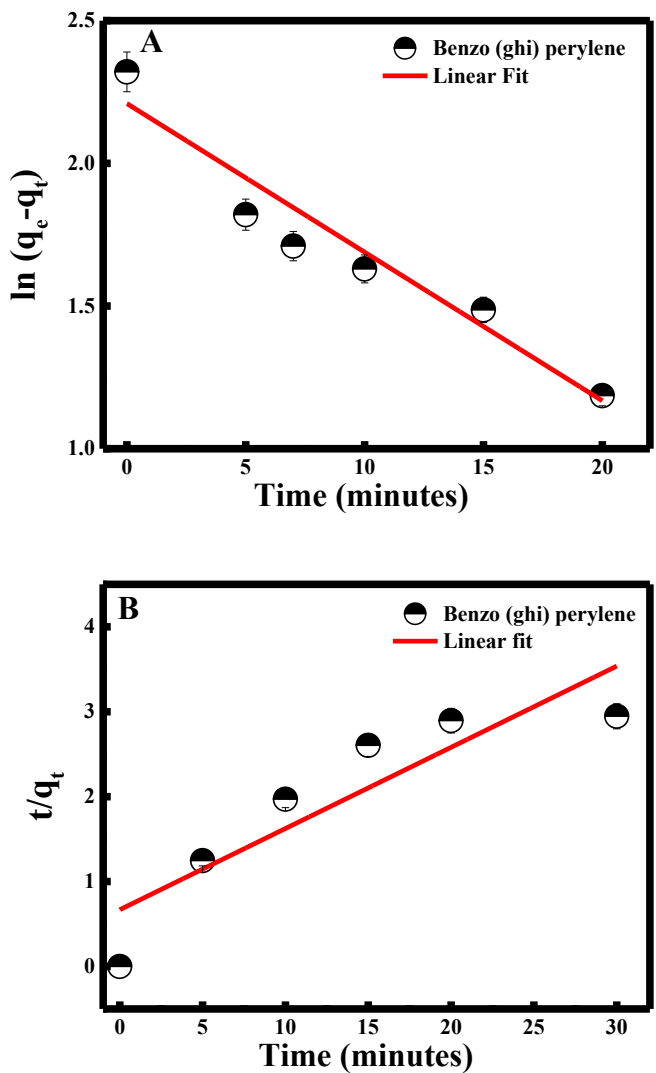
Figure 26 Benzo (ghi) perylene adsorption in (A)pseudo first order kinetic model and (B) pseudo second order kinetic model (n=3).

For the pseudo-first order kinetic model, a linear curve was obtained when plotting ln (q_e-q_t) vs. t (minutes) and the values of k_1 and q_e were calculated from the slope and intercept of the equation, shown below [114]:

$$\ln(qe - qt) = \ln qe - K1t \qquad (2)$$

Also, for the pseudo-second order kinetic model, a linear curve was also attained when plotting t/q_t vs. t (minutes) and k_2 was calculated from the intercept and q_e from the slope of the equation shown below:

$$\frac{t}{qt} = \frac{1}{qe} + K2t \quad (3)$$

where K_1, k_2 and q_e for the pseudo-first and pseudo-second order are summarized in Table 4.

According to the computational data, there is a notable difference in the R^2 value of the two kinetic models, with the pseudo-first order having the better value ($R^2 = 0.98 > R^2 = 0.76$).

Moreover, the adsorption capacity calculated in the pseudo-first kinetic model (9.11 mg/g) is the closest to the one found experimentally (10.18 mg/g).

These results show that the pseudo-first order kinetics took place in the adsorption process.

In fact, Pseudo-first order means that the adsorption is done by physisorption process which means that the SiO_2 NPs adsorbent and benzo(ghi)perylene adsorbate are bonding due to Van der Waals forces.

Adsorbent	Pseudo-first order			Pseudo-second order			q_e (calc) (mg/g)
	q_e (exp) (mg/g)	k_1 (min^{-1})	R^2	q_e (exp) (mg/g)	k_2 (g.mg^{-1}.min^{-1})	R^2	
SiO_2 NPs	9.11	-0.052	0.98	1.50	0.096	0.76	10.18

Table 4 Fitting results for pseudo first and pseudo second order kinetics analysis.

4. *Adsorption isotherms study*

The isothermal study for different benzo (ghi) perylene concentrations at a fixed dosage of SiO_2 NPs adsorbent equal to 10 mg was carried out in order to identify the isotherm model. Freundlich and Langmuir models are the two most commonly used

isotherms. Freundlich isotherm suggests that the adsorption takes place in a multi-layer way. This means that the adsorbent has infinite number of adsorption sites on the surface and that these sites have different energies. Freundlich isotherm is represented by the equation below [115]:

$$\ln qe = \ln Kf + \frac{1}{n} \ln Cf \quad (4)$$

where K_f is the Freundlich constant that indicates the adsorption capacity (amount of PAH adsorbed), $\frac{1}{n}$ is Freundlich constant that signifies the intensity of adsorption.

Hence, Figure 27 represents the plot of ln (q_e) versus ln (C_f). K_f and $\frac{1}{n}$ were calculated from the intercept and slope value respectively.
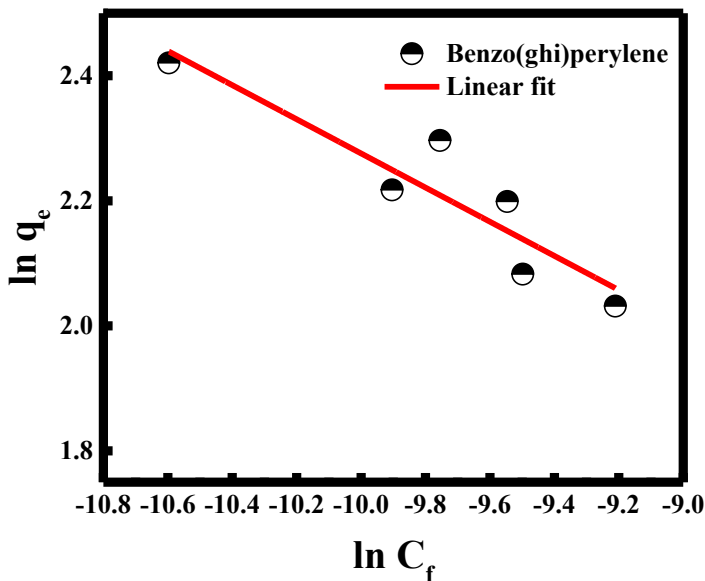
Figure 27 The Freundlich isotherm model (n=3).

However, Langmuir isotherm proposes that the adsorbent contains limited sites of adsorption on its surface and that these sites have the same energies, and that only one PAH compound could be adsorbed in each site.

Hence the adsorption mechanism that is taking place is monolayer and homogeneous. Langmuir isotherm is illustrated be the equation below [116]:

$$\frac{Ce}{qe} = \frac{1}{qm} Kl + \frac{Ce}{qm} \quad (5)$$

where q_m is the maximum adsorption capacity (mg/g), K_L is Langmuir constant that relates to the energy of adsorption. These two constants are calculated from the slope and intercept respectively when $\frac{Ce}{qe}$ is plotted against C_e (See Figure 28).
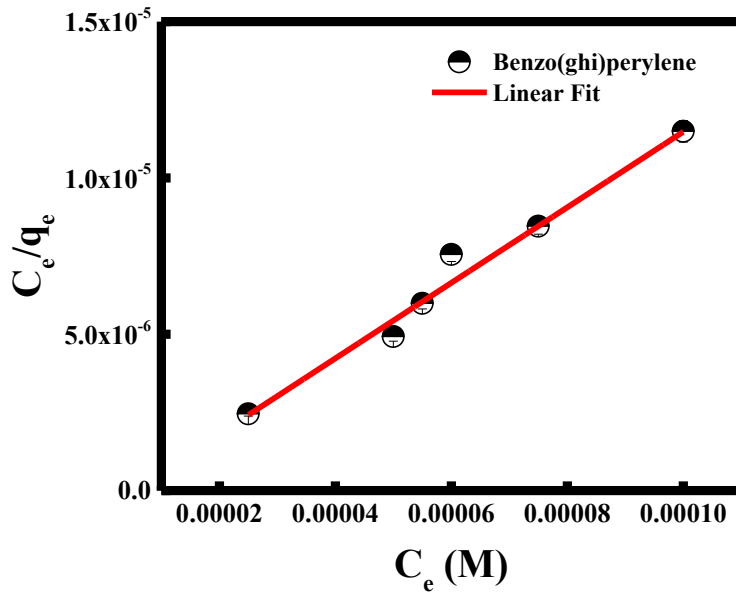
Figure 28 The Langmuir isotherm model (n=3).

Based on the results obtained, we can conclude that the adsorption of benzo(ghi)perylene onto SiO_2 NPs surface followed the Langmuir isotherm where the R^2 value obtained for Langmuir isotherm is much higher than the value obtained when adopting Freundlich isotherm (0.98>0.81). These results verify the presence of a monolayer adsorption onto a homogeneous surface (See Table 5).

Adsorbent	Langmuir isotherm			Freundlich isotherm		
	q_m (mg/g)	K_L	R^2	$\frac{1}{n}$	K_f	R^2
SiO$_2$ NPs	6.30	$-1.26*10^{-5}$	0.98	-0.25	0.76	0.81

Table 5 Isotherm study for benzo(ghi)perylene PAH.

5. *Thermodynamics study*

The thermodynamic parameters, the standard enthalpy change (ΔH^o), the entropy change (ΔS^o) and the standard free energy change (ΔG^o) were calculated. ΔH^o and ΔS^o were determined by using the van't Hoff equation (equations 6&7) and ΔG^o was valued using the thermodynamics equation (equation 8) [117].

$$\ln Keq = \frac{C_{ads}}{Ce} \qquad (6)$$

$$\ln K = \frac{\Delta S^o}{R} - \frac{\Delta H_o}{RT} \qquad (7)$$

$$\Delta G^o = \Delta H^o - T \, \Delta S^o \qquad (8)$$

where K_{eq} is the constant at equilibrium, C_{ads} is the amount of benzo(ghi)perylene adsorbate in mg/g, C_e is the concentration of benzo(ghi)perylene at equilibrium in mg/L, R is the constant of gas equal to 8.314 mol/K, and T is temperature of absolute solution in °K.

ΔH^o and ΔS^o are determined from the slope and intercept of the linear graph obtained when ln K is plotted against 1/T (See Figure 29).
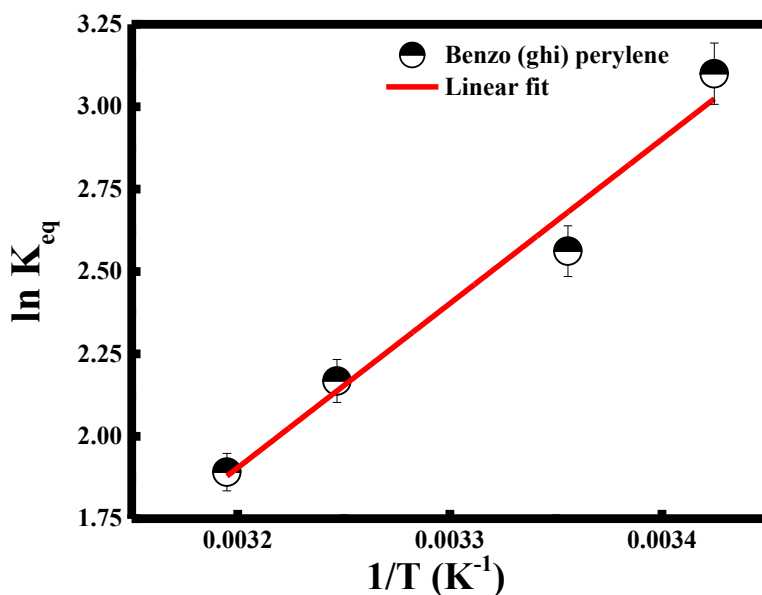
Figure 29 Van't Hoff plot for the adsorption of benzo(ghi)perylene (n=3).

According to the results found, we can conclude that the adsorption process taking place is exothermic since ΔH^o is negative and the entropy has decreased in liquid-solid interfaces since ΔS^o value is negative also (See Table 6).

Furthermore, the standard free energy change (ΔG^o) has also a negative value which means that this adsorption mechanism is spontaneous. And the value of ΔG^o (-7.34 kJ/mol) is in the range of $-20 < \Delta G^o < 0$ kJ/mol which indicates that the mechanism is a physisorption one.

Adsorbent	SiO$_2$ NPs
ΔH^o (kJ/mol)	-41.42
ΔS^o (J/mol K)	-116.7
ΔG^o (kJ/mol) at 292 K	-7.34
R^2	0.97

Table 6 Thermodynamics parameters for benzo(ghi)perylene onto SiO$_2$ NPs.

6. *Selectivity towards other organic compounds*

It was greatly important to study the selectivity of the adsorption process particularly in this new study.

Hence, different control experiments were done using acenaphthene, acenaphthylene, acetaminophen, anthracene, benzo(a)anthracene, benzo(a)pyrene, benzo(b)fluoranthene, chrysene, coronene, dibenzo(ah)anthracene, fluoranthene, indenol(1,2,3,cd)pyrene and naphthalene to test the selectivity of the adsorption process for benzo(ghi)perylene.

For this purpose, 500 µM stock solution of each PAH was used to complete the selectivity experiments. The adsorption capacity q_e was calculated for each PAH and shown in Figure 30.
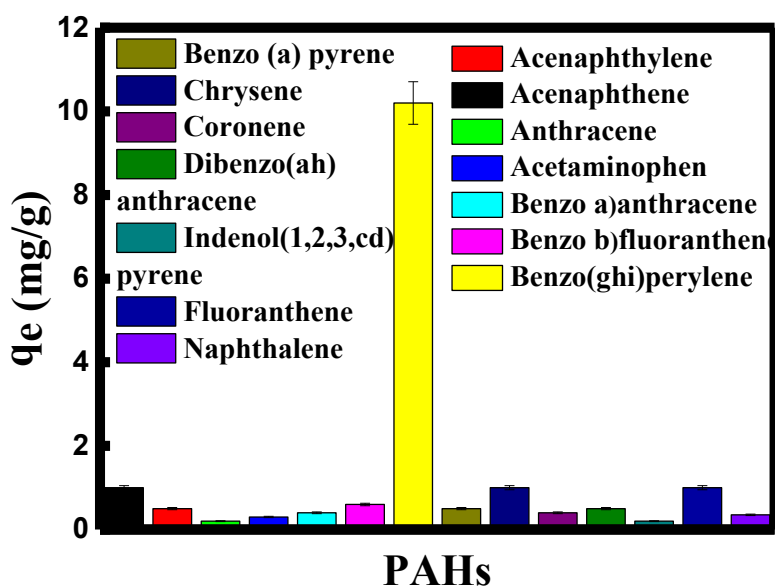
Figure 30 Adsorption capacity q_e of silica nanoparticles in the presence of 25 µM of different PAHs.

The maximum adsorption capacity value q_e didn't exceed a value of 1 mg/g when different PAHs were used. However, when benzo(ghi)perylene was added to the silica nanoparticles the q_e obtained was equal to 10.18 mg/g indicating that the adsorbent is selective towards the adsorbate benzo(ghi)perylene.

In addition, different organic dyes were tested to prove the high selectivity of these NPs in this work. Therefore, methylene blue, methyl orange, congo red, rhodamine B and rhodamine 6G were used and the maximum adsorption capacity was calculated. The highest q_e attained was found to be really minimal (2.1 mg/g for methylene blue) compared to the q_e obtained for benzo(ghi)perylene (10.18 mg/g). Thus, these results prove the high selectivity of SiO_2 NPs towards benzo(ghi)perylene.

7. *Characterization of silica nanoparticles after adsorption*

a) Surface area analysis (BET)

Surface area analysis (BET) was carried out next on a sample of silica nanoparticles before the addition of any benzo(ghi)perylene and on a sample of silica after the adsorption of benzo(ghi)perylene in order to see the modification done on the surface area of the silica nanoparticles.

BET results revealed that the surface area of the silica nanoparticles decreased from 111.9291 m^2/g before adsorption to 82.9364 m^2/g after the adsorption of benzo(ghi)perylene. This decrease of surface area verifies the adsorption process happening on the surface of the silica nanoparticles.

b) Thermogravimetric analysis (TGA)

Thermogravimetric analysis (TGA) was measured on a sample of silica after the adsorption of benzo(ghi)perylene in order to see how much mass this sample will lose. The TGA spectra is illustrated in Figure 31 where it shows that there is a % mass loss of ~30% for the sample of silica containing the PAH adsorbed. However, the % weight loss of a sample of silica was ~10%.

This high mass loss is attributed to the degradation of benzo(ghi)perylene from the surface of the silica nanoparticles hence its bigger value.
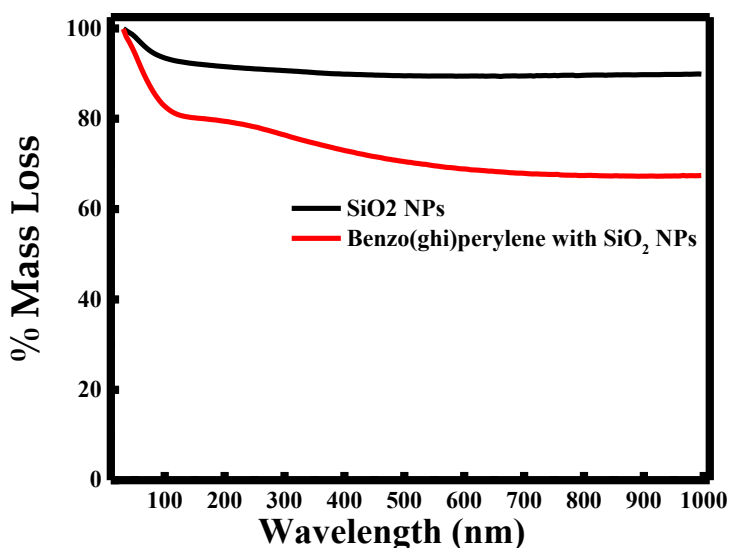
Figure 31 Thermogravimetric analysis (TGA) of SiO_2 NPs with and without benzo(ghi)perylene.

D. Conclusion

Silica nanoparticles were shown to be an efficient and highly selective adsorbent for benzo(ghi)perylene. Moreover, a satiated adsorption capacity of this PAH onto their surface at high concentration was observed the first ever to be found. There results were found without using any surfactant or modifying their chemistry surface.

The adsorption capacity increased with the increase of adsorbent dose with a q_e value equal to 10.18 mg/g. In contrary, q_e decreased with the increase of benzo(ghi)perylene concentration and reaching a value of 6.90 mg/g.

In addition, the pseudo-first order was the best kinetic model which indicates that physisorption was taking place. This also was proved when calculating the thermodynamics parameters of this adsorption process and acquiring a negative standard free energy change in the range $-20 < \Delta G^o < 0$ kJ/mol.

Finally, the isotherm study was completed to designate that the data experimentally found fit the Langmuir isotherm.

CHAPTER VI

CONCLUSION

Briefly, silica nanoparticles were synthesized using a simple process by sol-gel method that consisted of adding dropwise 1 mL of colloidal silica followed by 2 mL of NaOH (100 mM) to a mixture of 5 mL double distilled water and 5 mL of ethanol. The best precursor to use was colloidal silica and the most suitable concentration of NaOH was 100 mM due to the generation of the smallest and most stable nanoparticles when these two parameters were used.

The efficiency of SiO_2 NPs as being nanoprobe was in the first place proved by applying them in the detection of $AgNO_3$. The detection of silver ion was completed based on resonance Rayleigh scattering which is a simple, cheap and fast technique to use. Silica nanoparticles showed a linear relationship with the concentration of $AgNO_3$ being in the range 5-300 μM. The detection of Ag^+ ion was done based on an electrostatic interaction happening between the negatively charged surface of the nanoparticles and the positively charged ions. The selectivity of the nanoparticles was studied also and showed that SiO_2 NPs were highly selective towards Ag^+ in comparison to other ions that could interfere with silver. The percent recovery was between 98 and 100% and the limit of detection (LOD) was 130 nM.

Silica nanoparticles are widely known as being competent adsorbents for hazardous and toxic molecules. For this purpose, the efficacy of SiO_2 NPs as adsorbent for the removal of PAHs was established. In the first place, the adsorption mechanism of benzo(ghi)perylene using SiO_2 NPs was optimized by varying the adsorbent dose, PAH concentration, pH and temperature. Hence, the results showed that the adsorption

capacity q_e increased with the increase of adsorbent dosage and reached its maximum of 10.18 mg/g. In contrary, q_e decreased with the increase of benzo(ghi)perylene concentration to reach a value of 6.90 mg/g. The data fit the pseudo-first order and Langmuir model. In addition, the thermodynamic results were calculated and showed that the adsorption process taking place was a physisorption and that it was spontaneous.

In summary, silica nanoparticles have shown a large interest in the biomedical and environmental fields.

REFERENCES

[1] Bleeker, E.A.J. *et al.* (2013). "Considerations on the EU definition of a nanomaterial: Science to support policy making," *Regul. Toxicol. Pharmacol.* **65** (1): 119–125.

[2] Lidén, G. (2011). "The European commission tries to define nanomaterials." *Ann. Occup. Hyg.* **55** (1): 1–5.

[3] Willard, M.A.; Kurihara, L.K.; Carpenter, E.E.; Calvin, S.; Harris, V.G. (2004). "Chemically prepared magnetic nanoparticles." *Int. Mater. Rev.* **49** (3–4): 125–170.

[4] Larner, S.F.; Wang, J.; Goodman, J.; O'Donoghue Altman, M.B.; Xin, M.; Wang, K.K.W. (2017). "In vitro neurotoxicity resulting from exposure of cultured neural cells to several types of nanoparticles." *J. Cell Death*. **10** (11): 1–7.

[5] Lungu, M.; Neculae, A.; Bunoiu, M.; Biris, C. (2015). "Nanoparticles' promises and risks: Characterization, manipulation, and potential hazards to humanity and the environment." *Nanoparticles' Promises Risks Charact. Manip. Potential Hazards to Humanit. Environ.* (4): 1–355.

[6] Parveen S.; Misra R.; Sahoo S. (2012). "Nanoparticles: a boon to drug delivery, therapeutics, diagnostics and imaging." *Nanomedicine Nanotechnology, Biol. Med*. **8** (2): 147- 166.

[7] Park, S.K. ; Kim, K.D. ; Kim, H.T. (2002). "Preparation of silica nanoparticles : determination of the optimal synthesis conditions for small and uniform particles". *Colloids and Surfaces A*. **197** (1–3) : 7–17.

[8] Mieville, R.L. (1972). « Measurement of microporosity in the presence of mesopores." *Journal of Colloid and Interface Science.* **41** (2): 371-373.

[9] Inagaki S, Fukushima Y, Okada A, Kato C, Kuroda K, inventors; Toyota Central Research and Development Laboratories, Inc., Japan. assignee. Manufacture of layer-form silica-metal oxide porous intercalation compounds useful as adsorbents and catalysts patent JP04238810A. 1992.

[10] Beck, JS.; Vartuli, JC; Roth, WJ; Leonowicz, ME; Kresge, CT; Schmitt, KD; et al. (1992). "A new family of mesoporous molecular sieves prepared with liquid crystal templates." *J Am Chem Soc*. **114** (27):10834–10843.

[11] Prabha, S.; Durgalakshmi, D.; Rajendran, S.; Lichtfouse, E. (2020). "Plant-derived silica nanoparticles and composites for biosensors, bioimaging, drug delivery and supercapacitors: a review." *Environmental Chemistry Letters.* **19**: 1667-1691.

[12] Roggers, R.; Kanvinde, S.; Boonsith, S.; Oupický, D. (2014). "The Practicality of Mesoporous Silica Nanoparticles as Drug Delivery Devices and Progress Toward This Goal." *AAPS PharmSciTech*. **15** (5): 1163–1171.

[13] Abi Rahman I.; Padavettan V. (2012). "Synthesis of Silica Nanoparticles by Sol-Gel: Size-Dependent Properties, Surface Modification, and Applications in Silica-Polymer Nanocomposites—A Review". *Journal of Nanomaterials.* **2012**: 1-15.

[14] Hench, L.L.; West, J.K. (1990). "The Sol-Gel process." *Chemical Reviews*. **90** (1): 33–72.

[15] Malik, M.A; Wani, M.Y; Hashim, M.A. (2012). "Microemulsion method: A novel route to synthesize organic and inorganic nanomaterials: 1st Nano Update." *Arabian Journal of Chemistry.* **5** (4): 397-417.

[16] Bagwe, R.P; Yang, C; Hilliard, L.R; Tan, W. (2004). "Optimization of Dye-Doped Silica Nanoparticles Prepared Using a Reverse Microemulsion Method." *Langmuir.* **20** (19): 8336-8342.

[17] Lin, C.-H.; Chang, J.-H.; Yeh, Y.-Q.; Wu, S.-H.; Liu, Y.-H.; Mou, C.-Y. (2015). "Formation of hollow silica nanospheres by reverse microemulsion." *Nanoscale.* **7**(21): 9614–9626.

[18] Johannessen, T.; Jensen, J.R.; Mosleh, M.; Johansen, J.; Quaade, U.; Livbjerg, H. (2004). "FLAME SYNTHESIS OF NANOPARTICLES Applications in Catalysis and Product/Process Engineering." *Chemical Engineering Research and Design.* **82** (11): 1444-1452.

[19] Kammler, H.K.; Madler, L.; Pratsinis, S.E. (2001). "Flame Synthesis of Nanoparticles." *Chemical Engineering Technology.* **24** (6): 583-596.

[20] Yue, R.; Meng, D.; Ni, Y.; Jia, Y.; Liu, G.; Yang, J.; Liu, H.; Wu, X.; Chen, Y. (2013). "One-step flame synthesis of hydrophobic silica nanoparticles*." Powder Technology.* **235**: 909–913.

[21] Nakamura, H.; Matsui, Y. (1995). "Silica Gel Nanotubes Obtained by the Sol-Gel Method." *J. Am. Chem. Soc.* **117** (9): 2651-2652.

[22] Stöber, W.; Fink, A.; Bohn, E. (1968). "Controlled growth of monodisperse silica spheres in the micron size range." *J. Colloid Interface Sci.* **26**: 62–69.

[23] Rao, K.; El-Hami, K.; Kodaki, T.; Matsushige, K.; Makino, K. (2005). "A novel method for synthesis of silica nanoparticles". *Journal of Colloid and Interface Science.* **289**: 125-131.

[24] Wu, S.-H ; Mou, C.-Y.; Lin, H.-P. (2013). "Synthesis of mesoporous silica nanoparticles." *Chem. Soc. Rev.* **42**:3862.

[25] Zhao, Y.; Wang, Y.; Ran, F.; Cui, Y.; Liu, C.; Zhao, Q.; Gao, Y.; Wang, D.; Wang, S. (2017). "A comparison between sphere and rod nanoparticles regarding their *in vivo* biological behavior and pharmacokinetics." *Scientific Reports.* **7**: 4131.

[26] Selvarajan, V.; Obuobi, S.; Ee, P.L.R. (2020). "Silica nanoparticles – a versatile tool for the treatment of bacterial infections." *Front. Chem.*

[27] Li, J.; Shen, S.; Kong, F.; Jiang, T.; Tang, C.; Yin, C. (2018). "Effects of pore size on *in vitro* and *in vivo* anticancer efficacies of mesoporous silica nanoparticles." *RSC Adv.* **8**: 24633–24640.

[28] Teolato, P.; Rampazzo, E.; Arduini, M.; Mancin, F.; Tecilla, P.; Tonellato, U. (2007). "Silica Nanoparticles for Fluorescence Sensing of ZnII: Exploring the Covalent Strategy." *Chemistry - A European Journal.* **13**(8): 2238–2245.

[29] Arreche, R.; Blanco, M.; Vázquez, P.; Martin-Martinez, J.M. (2011). "Use of new silica fillers as additives for polymers used in packaging of fruit." *Quim Nova.* **35** (10): 1907-1911.

[30] Zhuang, C.; Chen, Y. (2019). "The effect of nano-SiO$_2$ on concrete properties: a review." *Nanotechnology Reviews.* **8** (1).

[31] Muller, U.; Reck, B.; Roser, J.; inventors; Basf Aktiengesellschaft, Germany. assignee. (1998). Mesoporous silica and its preparation for use as catalysts or supports for catalysts, drugs, enzymes or pigments patent.

[32] Schuth, F.; Ciesla, U.; Schacht, S.; Thieme, M.; Huo, Q.; Stucky, G. (1999). "Ordered mesoporous silicas and zirconias: control on length scales between nanometer and micrometer." *Mater Res Bull.* **34** (3):483–494.

[33] Balkus, KJ. Jr.; Coutinho, D.; Lucas, J.; Washmon-Kriel, L. (2001). "Synthesis and characterization of DAM-1 type materials." *Mater Res Soc Symp Proc.* 628(Organic/Inorganic Hybrid Materials):CC10.7.1-CC.7.6.

[34] Kaiser, C.; Buchel, G.; Ludtke, S.; Lauer, I.; Unger, KK. (1997). "Processing of microporous/mesoporous submicron-size silica spheres by means of a template-supported synthesis." *Spec Publ - R Soc Chem.* 213: 406–412.

[35] González, B.; Colilla, M.; Díez, J.; Pedraza, D.; Guembe, M.; Izquierdo- Barba; I., et al. (2018). "Mesoporous silica nanoparticles decorated with polycationic dendrimers for infection treatment." *Acta Biomater.* 68: 261–271.

[36] Kavruk, M.; Celikbicak, O.; Ozalp, V. C.; Borsa, B. A.; Hernandez, F. J.; Bayramoglu, G.; et al. (2015). "Antibiotic loaded nanocapsules functionalized with aptamer gates for targeted destruction of pathogens." *Chem. Commun.* 51: 8492–8495.

[37] Yang, Y.; Yu, C. (2016). "Advances in silica-based nanoparticles for targeted cancer therapy." *Nanomedicine: Nanotechnology, Biology and Medicine.* 12 (2): 317–332.

[38] Brezaniova, I.; Zaruba, K.; Kralova, J.; Sinica, A.; Adamkova, H.; Ulbrich, P.; Pouckova, P.; Hruby, M.; Stepanek, P.; Kral, V. (2018). "Silica-based nanoparticles are efficient delivery systems for temoporfin." *Photodiagnosis and photodynamic therapy.* 21: 275-284.

[39] Chaudhary, Z.; Subramaniam, S.; Khan, G.M.; Abeer, M.M.; Qu, Z.; Janjua, T.; Kumeria, T.; Batra, J.; Popat, A. (2019). "Encapsulation and Controlled Release of Resveratrol Within Functionalized Mesoporous Silica Nanoparticles for Prostate Cancer Therapy." *Frontiers in Bioengineering and Biotechnology.* 7: 225.

[40] Jadhav, S. A.; Garud, H. B.; Patil, A. H.; Patil, G. D.; Patil, C. R.; Dongale, T. D.; Patil, P. S. (2019). "Recent advancements in silica nanoparticles-based technologies for removal of dyes from water." *Colloid and Interface Science Communications.* 30: 100181.

[41] Raj, S. I.; Jaiswal, A.; Uddin, I. (2019). "Tunable porous silica nanoparticles as a universal dye adsorbent." *RSC Advances.* 9 (20): 11212–11219.

[42] Qin, P.; Yang, Y.; Zhang, X.; Niu, J.; Yang, H.; Tian, S.; Zhu, J.; Lu, M. (2017). "Highly Efficient, Rapid, and Simultaneous Removal of Cationic Dyes from Aqueous Solution Using Monodispersed Mesoporous Silica Nanoparticles as the Adsorbent." *Nanomaterials.* 8 (1): 4.

[43] Shinde, P.S.; Suryawanshi, P.S.; Patil, K.K.; Belekar, V.M.; Sankpal, S.A.; Delekar, S.D.; Jadhav, S.A. (2021). "A Brief Overview of Recent Progress in Porous Silica as Catalyst Supports." *J. Compos. Sci.* 5: 75.

[44] Dickschat, A. T.; Behrends, F.; Surmiak, S.; Weiß, M.; Eckert, H.; Studer, A. (2013). "Bifunctional mesoporous silica nanoparticles as cooperative catalysts for the Tsuji–Trost reaction – tuning the reactivity of silica nanoparticles." *Chemical Communications.* 49 (22): 2195.

[45] Yang, X.; Chen, D.; Liao, S.; Song, H.; Li, Y.; Fu, Z.; Su, Y. (2012). "High-performance Pd–Au bimetallic catalyst with mesoporous silica nanoparticles as support and its catalysis of cinnamaldehyde hydrogenation." *Journal of Catalysis.* 291: 36–43.

[46] Nishimura, H.; Ritchie, K.; Kasai, R. S.; Goto, M.; Morone, N.; Sugimura, H.; et al. (2013). "Biocompatible fluorescent silicon nanocrystals for singlemolecule tracking and fluorescence imaging." *J. Cell Biol.* 202: 967–983.

[47] Park, J. H.; Gu, L.; von Maltzahn, G.; Ruoslahti, E.; Bhatia, S. N.; Sailor, M. J. (2009). "Biodegradable luminescent porous silicon nanoparticles for in vivo applications." *Nat. Mater.* **8**: 331–336.

[48] Sung, T.W.; Lo, Y.L. (2012). "Highly sensitive and selective sensor based on silica-coated CdSe/ZnS nanoparticles for Cu^{2+} detection." *Sensors and Actuators B.* **165**: 119-125.

[49] Tan, S. Y.; Teh, C.; Ang, C. Y.; Li, M.; Li, P.; Korzh, V.; Zhao, Y. (2017). "Responsive mesoporous silica nanoparticles for sensing of hydrogen peroxide and simultaneous treatment toward heart failure." *Nanoscale.* **9** (6): 2253–2261.

[50] Santra, S.; Yang, H.; Dutta, D.; Stanley, J. T.; Holloway, P. H.; Tan, W.; Moudgil, B.M.; Mericle, R. A. (2004). "TAT conjugated, FITC doped silica nanoparticles for bioimaging applications." *Chemical Communications.* (24): 2810.

[51] Cha, B. G.; Kim, J. (2018). "Functional mesoporous silica nanoparticles for bio-imaging applications." *Wiley Interdisciplinary Reviews: Nanomedicine and Nanobiotechnology. e1515.*

[52] Santra, S.; Bagwe, R. P.; Dutta, D.; Stanley, J. T.; Walter, G. A.; Tan, W.; Moudgil, B.M.; Mericle, R. A. (2005). "Synthesis and Characterization of Fluorescent, Radio-Opaque, and Paramagnetic Silica Nanoparticles for Multimodal Bioimaging Applications." *Advanced Materials.* **17** (18): 2165–2169.

[53] A. M. Ealias; M. P. Saravanakumar. (2017). "A review on the classification, characterisation, synthesis of nanoparticles and their application." *IOP Conf. Ser. Mater. Sci. Eng.* **263**: 1–15.

[54] Haynes, W. M.; Lide, D. R.; Bruno, T. J. (2016-2017). "Abundance of Elements in the Earth's Crust and in the Sea." *CRC.*

[55] Heaney, P. J. (1994). "Structure and chemistry of the lowpressure silica polymorphs." *Rev. Mineral. Geochem.* **29**: 1–40.

[56] Iler, R. K. (1979). "The Chemistry of Silica: Solubility, Polymerization, Colloid and Surface Properties and Biochemistry of Silica." *Wiley.*

[57] Croissant, J.G.; Butler, K.S.; Zink, J.I.; Brinker, C. J. (2020). "Synthetic amorphous silica nanoparticles: toxicity, biomedical and environmental implications." *Nature Reviews Materials.*

[58] Castillo, R. R. et al. (2019). "Advances in mesoporous silica nanoparticles for targeted stimuli-responsive drug delivery: an update." *Expert Opin. Drug Deliv.* **16**: 415–439.

[59] Hao, N.; Yang, H.; Li, L.; Li, L.; Tang, F. (2014). "The shape effect of mesoporous silica nanoparticles on intracellular reactive oxygen species in A375 cells." *New J. Chem.* **38**: 4258-4266.

[60] Zhao, Z. Y.; Liu, J.; Hahn, M.; Qiao, S. Z.; Middelberg, A. P. J.; He, L. Z. (2013). "Encapsulation of lipase in mesoporous silica yolk–shell spheres with enhanced enzyme stability." *RSC Advances.* **3**: 22008-22013.

[61] Knezevic, N.Z.; Ruiz-Hernandez, E.; Hennink, W.E.; Vallet-Regi, M. (2013). "Magnetic mesoporous silica-based core/shell nanoparticles for biomedical applications." *RSC Advances.* **3**: 9584-9593.

[62] Nallathambi, G.; Ramachandran, T.; Rajendran, V.; Palanivelu, R. (2011). "Effect of Silica Nanoparticles and BTCA on Physical Properties of Cotton Fabrics." *Materials Research.* **14** (4): 552-559.

[63] Jr, C.P.P. (2004). "Encyclopedic dictionary of condensed matter physics." *Academic Press.*

[64] Christopher, P.; Xin, H.; Linic, S. (2011). "Visible-light-enhanced catalytic oxidation reactions on plasmonic silver nanostructures." *Nat. Chem.* **3**(6): 467-472.

[65] Wu, H.; Kong, D.; Ruan, Z.; Hsu, P.; Wang, S.; Yu, Z.; Carney, T.J.; Hu, L.; Fan, S.; Cui, Y. (2013). "A transparent electrode based on a metal nanotrough network." *Nat. Nanotechnology.* **8**: 421-425.

[66] Chernousova, S.; Epple, M. (2013). "Silver as antibacterial agent: ion, nanoparticle, and metal." *Angew. Chem. Int. Ed.* **52**(6): 1636-1653.

[67] Arora, S.; Lidor, A.; Abularrage, C.J.; Weiswasser, J.M.; Nylen, E.; Kellicut, D.; Sidawy, A.N. (2006). "Thiamine (vitamin B1) improves endothelium-dependent vasodilatation in the presence of hyper- glycemia." *Ann Vasc Surg.* **20** (5):653–658.

[68] Wygladacz, K.; Radu, A.; Xu, C.; Qin, Y.; Bakker, E. (2005). "Fiber-optic microsensor array based on fluorescent bulk optode microspheres for the trace analysis of silver ions." *Anal Chem.* **77** (15): 4706–4712.

[69] Drake, P.L.; Hazelwood, K. J. (2005). "Exposure-Related Health Effects of Silver and Silver Compounds: A Review." *The Annals of Occupational Hygiene.* **49**(7): 575-585.

[70] López-López, J.A.; Jönsson, J.A.; García-Vargas, M.; Moreno, C. (2014). "Simple hollow fiber liquid membrane based pre-concentration of silver for atomic absorption spectrometry." *Analytical Methods.* **6** (5): 1462–1467.

[71] López-López, J.A.; Herce-Sesa, B.; Moreno, C. (2016). "Solvent bar micro-extraction with graphite atomic absorption spectrometry for the determination of silver in ocean water." *Talanta.* **159**: 117–121.

[72] Balcaen, L.; Bolea-Fernandez, E.; Resano, M.; Vanhaecke, F. (2015). "Inductively coupled plasma–Tandem mass spectrometry (ICP-MS/MS): a powerful and universal tool for the interference-free determination of (ultra)trace elements—a tutorial review." *Analytica Chimica Acta.* **894**: 7–19.

[73] Ramos, K.; Ramos, L.; Gómez-Gómez, M.M. (2017). "Simultaneous characterisation of silver nanoparticles and determination of dissolved silver in chicken meat subjected to in vitro human gastrointestinal digestion using single particle inductively coupled plasma mass spectrometry." *Food Chemistry.* **221**: 822–828.

[74] Lai, C.-Z.; Fierke, M.A.; da Costa, R.C.; Gladysz, J.A.; Stein, A.; Bühlmann, P. (2010). "Highly selective detection of silver in the low ppt range with ion-selective electrodes based on ionophore-doped fluorous membranes." *Analytical Chemistry.* **82** (18): 7634–7640.

[75] Kim, H.N.; Ren, W.X.; Kim, J.S.; Yoon, J. (2012). "Fluorescent and colorimetric sensors for detection of lead, cadmium, and mercury ions." *Chemical Society Reviews.* **41** (8): 3210-3244.

[76] Quang, D.T.; Kim, J.S. (2010). "Fluoro- and chromogenic chemodosimeters for heavy metal ion detection in solution and biospecimens." *Chemical Reviews*. **110 (**10): 6280–6301.

[77] van Zee, R.D.; Pomrenke, G.S. (2009). "Nanotechnology-Enabled Sensing." *Rep. Natl. Nanotechnol. Initiat. Work.* [Online].

[78] Cooper, T.A.; Wan, L.; Dreyfuss, G. (2009). "RNA and Disease." *Hhmi*. **136** (4): 777–793.

[79] Cullum, B.M.; Vo-dinh, T. (1938). "The development of optical biosensors for Biological Measurement." *Bmj*. **1** (4017): 20–21.

[80] Tan, S.Y.; Teh, C.; Ang, C.Y.; Li, M.; Li, P.; Korzh, V.; Zhao, Y. (2017). "Responsive mesoporous silica nanoparticles for sensing of hydrogen peroxide and simultaneous treatment toward heart failure." *Nanoscale*. **9**: 2253-2261.

[81] El-Kurdi, R.; Patra, D. (2019). "Gold and silver nanoparticles in resonance Rayleigh scattering techniques for chemical sensing and biosensing: a review." *Microchimica Acta*. **186**: 667.

[82] Yan, S.; Deng, D.; Li, L.; Chen, Y.; Song, H.; Lv, Y. (2016). "Glutathione modified Ag_2Te nanoparticles as a resonance Rayleigh scattering sensor for highly sensitive and selective determination of cytochrome C." *Sens. Actuators B Chem.* **228**: 458-464.

[83] Jafari, S.; Derakhshankhah, H.; Alaei, L.; Fattahi, A.; Varnamkhasti, B.S.; Saboury, A.A. (2019). "Mesoporous silica nanoparticles for therapeutic/diagnostic applications." *Biomedicine & Pharmacotherapy*. **109**: 1100-1111.

[84] Eftekhari, M.; Schwarzenberger, K.; Javadi, A.; Eckert, K. (2020). "The influence of negatively charged silica nanoparticles on the surface properties of anionic surfactants: electrostatic repulsion or the effect of ionic strength?" *Phys. Chem. Chem. Phys.* **22**: 2238-2248.

[85] Li, Y.; Yan, J.; Xu, Z. (2019). "A Sensitive Fluorescence Biosensor for Silver Ions (Ag+) Detection Based on C-Ag+-C Structure and Exonuclease III-Assisted Dual-Recycling Amplification." *Journal of Analytical Methods in Chemistry*. **2019**.

[86] Gao, Z.; Liu, G.G.; Ye, H.; Rauschendorfer, R.; Tang, D.; Xia, X. (2017). "Facile Colorimetric Detection of Silver Ions with Picomolar Sensitivity." *Anal. Chem.* **89:** 3622-3629.

[87] Hatai, J.; Pal, S.; Bandyopadhyay, S. (2012). "Fluorescent detection of silver ions in water with organic nano-aggregates." *RSC Advances*. **2:** 10941-10947.

[88] Jang, K.; You, J.; Park, C.; Na, S. (2017). "Highly sensitive detection of silver ions using a silver-specific DNA based nano-porous micro-resonator." *New Journal of Chemistry*. **41** (4): 1840-1845.

[89] Selva Sharma, A.; SasiKumar, T.; Ilanchelian, M. (2018). "A Rapid and Sensitive Colorimetric Sensor for Detection of Silver Ions Based on the Non-aggregation of Gold

Nanoparticles in the Presence of Ascorbic Acid." *Journal of Cluster Science.* **29** (4): 655-662.

[90] Blumer, M.; Blumer, W.; Reich, T. (1977). "Polycyclic aromatic hydrocarbons in soils of a mountain valley: Correlation with highway traffic and cancer incidence." *Environmental Science and Technology.* **11**: 1082–1084.

[91] Vichi, S.; Pizzale, L.; Conte, L. S.; Buxaderas, S.; LópezTamames, E. (2005). "Simultaneous determination of volatile and semi-volatile aromatic hydrocarbons in virgin olive oil by headspace solid-phase microextraction coupled to gas chromatography/mass spectrometry." *Journal of Chromatography A.* **1090**: 146–154.

[92] Haritash, A. K.; Kaushik, C. P. (2009). "Biodegradation aspects of Polycyclic Aromatic Hydrocarbons (PAHs): A review." *Journal of Hazardous Materials.* **169**(1–3): 1–15.

[93] Kuppusamy, S.; Thavamani, P.; Megharaj, M.; Naidu, R. (2016). "Biodegradation of polycyclic aromatic hydrocarbons (PAHs) by novel bacterial consortia tolerant to diverse physical settings - Assessments in liquid- and slurryphase systems." *International Biodeterioration and Biodegradation.* **108**: 149–157.

[94] Li, P. H.; Wang, Y.; Li, Y. H.; Wai, K. M.; Li, H. L.; Tong, L. (2016). "Gas-particle partitioning and precipitation scavenging of polycyclic aromatic hydrocarbons (PAHs) in the free troposphere in southern China." *Atmospheric Environment.* **128**: 165–174.

[95] Harvey, R. G. (1997). "Polycyclic aromatic hydrocarbons." *New York, NY: Wiley-VCH.*

[96] Zhang, Y.; Cui, B.; Zhang, Q.; Liu, X. (2015). "Polycyclic aromatic hydrocarbons in the food web of Coastal Wetlands: Distribution, sources and potential toxicity." *Clean - Soil, Air, Water.* **43**: 881–891.

[97] Armstrong, B. G.; Hutchinson, E.; Unwin, J.; Fletcher, T. (2004). "Lung cancer risk after exposure to polycyclic aromatic hydrocarbons: A review and meta-analysis." *Environ Health Perspect.* **112**: 970–978.

[98] Haritash, A. K.; Kaushik, C. P. (2009). "Biodegradation aspects of Polycyclic Aromatic Hydrocarbons (PAHs): A review." *Journal of Hazardous Materials.* **169**(1–3): 1–15.

[99] Szulejko, J. E.; Kim, K.-H.; Brown, R. J. C.; Bae, M.-S. (2014). "Review of progress in solvent-extraction techniques for the determination of polyaromatic hydrocarbons as airborne pollutants." *TrAC Trends in Analytical Chemistry.* **61**: 40–48.

[100] Zhou, Q.; Gao, Y. (2014). "Determination of polycyclic aromatic hydrocarbons in water samples by temperaturecontrolled ionic liquid dispersive liquid-liquid microextraction combined with high performance liquid chromatography." *Analytical Methods.* **6**: 2553–2559.

[101] Das, P.; Mukherjee, S.; Sen, R. (2008). "Improved bioavailability and biodegradation of a model polyaromatic hydrocarbon by a biosurfactant producing bacterium of marine origin." *Chemosphere.* **72**: 1229–1234.

[102] Xu, S. N.; Zhao, Q.; He, H. B.; Yuan, B. F.; Feng, Y. Q.; Yu, Q. W. (2014). "Rapid determination of polycyclic aromatic hydrocarbons in environmental water based on magnetite nanoparticles/polypyrrole magnetic solidphase extraction." *Analytical Methods.* **6**: 7046–7053.

[103] Cherng, S. H.; Lin, P.; Yang, J. L.; Hsu, S. L.; Lee, H. (2001). "Benzo[g,h,i] perylene synergistically transactivates benzo[a]pyrene- induced CYP1A1 gene

expression by aryl hydrocarbon receptor pathway." *Toxicology and Applied Pharmacology*. **170**(1): 63–68.

[104] Ewa, B.; Danuta, M. Š. (2017). "Polycyclic aromatic hydrocarbons and PAH-related DNA adducts." *Journal of Applied Genetics*. **58**(3): 321–330.

[105] Platt, K. L.; Grupe, S. (2005). "Microsomal biotransformation of benzo [ghi]perylene, a mutagenic polycyclic aromatic hydrocarbon without a "classic" bay region." *Chemical Research in Toxicology*. **18**(4): 700–710.

[106] Amador- Muñoz, O.; Bazán- Torija, S.; Villa- Ferreira, S. A.; Villalobos-Pietrini, R.; Bravo- Cabrera, J. L.; Munive- Colín, Z.; … Murillo- Tovar, M. A. (2013). "Opposing seasonal trends for polycyclic aromatic hydrocarbons and PM10: Health risk and sources in southwest Mexico City." *Atmospheric Research*. **122**: 199–212.

[107] Gao, B.; Guo, H.; Wang, X. M.; Zhao, X. Y.; Ling, Z. H.; Zhang, Z.; Liu, T. Y. (2012). "Polycyclic aromatic hydrocarbons in PM2.5 in Guangzhou, southern China: Spatiotemporal patterns and emission sources." *Journal of Hazardous Materials*. **239-240**: 78–87.

[108] Deutsch- Wenzel, R. P.; Brune, H.; Grimmer, G.; Dettbarn, G.; Misfeld, J. (1983). "Experimental studies in rat lungs on the carcinogenicity and dose- response relationships of eight frequently occurring environmental polycyclic aromatic hydrocarbons." *Journal of the National Cancer Institute*. **71**(3): 539–544.

[109] Hughes, N. C.; Phillips, D. H. (1993). "32P- postlabelling analysis of the covalent binding of benzo[ghi]perylene to DNA in vivo and in vitro." *Carcinogenesis*. **14**(1): 127–133.

[110] Van Duuren, B. L.; Goldschmidt, B. M. (1976). "Cocarcinogenic and tumor-promoting agents in tobacco carcinogenesis." *Journal of the National Cancer Institute*. **56**(6): 1237–1242.

[111] Gibson, L.T. (2014). "Mesosilica materials and organic pollutant adsorption: part B removal from aqueous solution." *Chem. Soc. Rev.* **43**: 5173-5182.

[112] Thomas, O.; Brogat, M. (2017). "Organic Constituents." *UV-Visible Spectrometry of Water and Wastewater.*

[113] Garba, Z.N.; Zhou, W.; Lawan, I.; Xiao, W.; Zhang, M.; Wang, L.; Chen, L.; Yuan, Z. (2019). "An overview of chlorophenols as contaminants and their removal from wastewater by adsorption: a review." *J. Environ. Manag.* **241**: 59-75.

[114] Kulkarni, M.R.; Revanth, T.; Acharya, A.; Bhato, P. (2017). "Removal of Crystal Violet dye from aqueous solution using water hyacinth: equilibrium, kinetics and thermodynamics study." *Resource-Efficient Technologies*. **3**: 71-77.

[115] Alshabanat, M.; Al-Mufarij, R.; Al-Senani, G. (2016). "Study on Adsorption of Malachite Green by Date Palm Fiber." *Orient. J. Chem.* **32** (6): 3139-3144.

[116] Alsenani, G. (2014). "Removal of Congo red dye from aqueous solution by date palm leaf base." *Am. J. Appl. Sci.* **11** (9): 1553-1557.

[117] Moaweda, E.A.; El-Shahat M.F. (2016). "Kinetic and thermodynamic studies of the removal of triphenyl methane dyes from wastewater using iodopolyurethane powder." *J. Taibah Univ. Sci. Sci. Direct Equilibrium.* **10**: 46-55.